



1 **Assessing impacts of selective logging on water,**  
2 **energy, and carbon budgets and ecosystem dynamics**  
3 **in Amazon forests using the Functionally Assembled**  
4 **Terrestrial Ecosystem Simulator**

5

6 Maoyi Huang<sup>1\*</sup>, Yi Xu<sup>1,2</sup>, Marcos Longo<sup>3,4</sup>, Michael Keller<sup>3,4,5</sup>, Ryan Knox<sup>6</sup>, Charles Koven<sup>6</sup>,  
7 Rosie Fisher<sup>7</sup>

8

9 <sup>1</sup>Atmospheric Sciences and Global Change Division, Pacific Northwest National Laboratory, Richland, WA, USA

10 <sup>2</sup>School of Geography, Nanjing Normal University, Nanjing, China

11 <sup>3</sup>Embrapa Agricultural Informatics, Campinas, SP, Brazil

12 <sup>4</sup>Jet Propulsion Laboratory, California Institute of Technology, Pasadena, CA, USA

13 <sup>5</sup>International Institute of Tropical Forestry, USDA Forest Service, Rio Piedras, Puerto Rico, USA

14 <sup>6</sup>Earth & Environmental Sciences Division, Lawrence Berkeley National Laboratory, Berkeley, CA, USA

15 <sup>7</sup>Climate and Global Dynamics Laboratory, National Center for Atmospheric Research, Boulder, CO, USA

16

17

18 *Correspondence to:* Maoyi Huang ([Maoyi.Huang@pnnl.gov](mailto:Maoyi.Huang@pnnl.gov))

19

20



21 **Abstract**

22 Tropical forest degradation from logging, fire, and fragmentation not only alters carbon stocks and  
23 carbon fluxes, but also impacts physical land-surface properties such as albedo and roughness  
24 length. Such impacts are poorly quantified to date due to difficulties in accessing and maintaining  
25 observational infrastructures, and the lack of proper modeling tools for capturing the interactions  
26 among biophysical properties, ecosystem demography, canopy structure, and biogeochemical  
27 cycling in tropical forests. As a first step to address these limitations, we implemented a selective  
28 logging module into the Functionally Assembled Terrestrial Ecosystem Simulator (FATES) by  
29 mimicking the ecological, biophysical, and biogeochemical processes following a logging event.  
30 The model can specify the timing and aerial extent of logging events, splitting the logged forest  
31 patch into disturbed and intact patches, determine the survivorship of cohorts in the disturbed  
32 patch, and modifying the biomass and necromass (total mass of coarse woody debris and litter)  
33 pools following logging. We parameterized the logging module to reproduce a selective logging  
34 experiment at the Tapajós National Forest in Brazil and benchmarked model outputs against  
35 available field measurements. Our results suggest that the model permits the coexistence of early  
36 and late successional functional types and realistically characterizes the seasonality of water and  
37 carbon fluxes and stocks, the forest structure and composition, and the ecosystem succession  
38 following disturbance. However, the current version of FATES overestimates water stress in the  
39 dry season therefore fails to capture seasonal variation in latent and sensible heat fluxes.  
40 Moreover, we observed a bias towards low stem density and leaf area when compared to  
41 observations, suggesting that improvements are needed in both carbon allocation and  
42 establishment of trees. The effects of logging were assessed by different logging scenarios to  
43 represent reduced impact and conventional logging practices, both with high and low logging  
44 intensities. The model simulations suggest that in comparison to old-growth forests the logged  
45 forests rapidly recover water and energy fluxes in one to three years. In contrast, the recovery times  
46 for carbon stocks, forest structure and composition are more than 30 years depending on logging  
47 practices and intensity. This study lays the foundation to simulate land use change and forest  
48 degradation in FATES, which will be an effective tool to directly represent forest management  
49 practices and regeneration in the context of Earth System Models.



## 50 1 Introduction

51 Land cover and land use in tropical forest regions are highly dynamic, and nearly all tropical forests  
52 are subject to significant human influence (*Martínez-Ramos et al.*, 2016; *Dirzo et al.*, 2014). While  
53 old-growth tropical forests have been reported to be carbon sinks that remove carbon dioxide from  
54 the atmosphere through photosynthesis, these forests could easily become carbon sources once  
55 disturbed (*Luysaert et al.*, 2008). Using data from forest inventory and long-term ecosystem  
56 carbon studies from 1990 to 2007, *Pan et al.* (2011) suggested a net tropical forest land-use source  
57 of  $1.3 \pm 0.7 \text{ Pg C yr}^{-1}$ , consisting of a gross tropical deforestation loss of  $2.9 \pm 0.5 \text{ Pg C yr}^{-1}$  that  
58 is partially offset by a carbon uptake by tropical secondary forest regrowth of  $1.6 \pm 0.5 \text{ Pg C yr}^{-1}$ .  
59 These estimates, however, do not account for tropical forest that has been degraded through the  
60 combined effects of selective logging (cutting and removal of merchantable timber), fuelwood  
61 harvest, understory fires, and fragmentation (*Nepstad et al.*, 1999; *Bradshaw et al.*, 2009). To date,  
62 the effects of forest degradation remain poorly quantified. Recent studies suggested that  
63 degradation may contribute to carbon loss 40% as large as clear cut deforestation (*Berenguer et*  
64 *al.*, 2014), and the emission from selective logging alone could be equivalent to ~10% to 50% of  
65 that from deforestation in the tropical countries (*Pearson et al.*, 2014; *Huang and Asner*,  
66 2010; *Asner et al.*, 2009). Selective logging of tropical forests is as an important contributor to  
67 many local and national economies, and correspond to approximately one eighth of global timber  
68 (*Blaser et al.*, 2011). The integrated impact of timber production and other forest uses has been  
69 posited as the cause of up to ~30% of the difference between potential and actual biomass stocks  
70 globally, comparable in magnitude to the effects of deforestation (*Erb et al.* (2017)).

71 Over half of all tropical forests have been cleared or logged, and almost half of standing old-  
72 growth tropical forests are designated by national forest services for timber production (*Sist et al.*,  
73 2015). Disturbances that result from logging are known to cause forest degradation at the same  
74 magnitude as deforestation each year in terms of both geographic extent and intensity, with  
75 widespread collateral damage to remaining trees, vegetation and soils, leading to disturbance to  
76 water, energy, and carbon cycling, as well as ecosystem integrity (*Keller et al.*, 2004b; *Asner et al.*,  
77 2004; *Huang and Asner*, 2010).

78 In most Earth system models (ESMs) that couple terrestrial to atmospheric processes to  
79 investigate global change selective logging is typically represented as simple fractions of affected  
80 area or an amount of carbon to be removed on a coarse grid (e.g., 0.5 degree). One exception is



81 the representation wood harvest in the LM3V land model that explicitly accounts for post-  
82 disturbance land age distribution, as part of the Geophysical Fluid Dynamics Laboratory (GFDL)  
83 Earth system model (Shevliakova et al., 2009). Grid cell fractional areas are typically based on  
84 timber production rates estimated from sawmill, sales, and export statistics (Hurtt et al.,  
85 2011; Lawrence et al., 2012). This approach, while practical, does not effectively differentiate  
86 selective logging that retains forest cover from deforestation. Selective logging includes cutting  
87 large trees and additional degradation through widespread damage to remaining trees, sub-canopy  
88 vegetation, and soils (Asner et al., 2004; Asner et al., 2005). Selective logging accelerates gap-  
89 phase regeneration within the degraded forests (Huang et al., 2008).

90 Such a simplified representation of wood harvest in ESMs has been necessary because models  
91 generally do not represent the demographic structure of forests (tree size and stem number  
92 distributions) (Bonan, 2008). But progress over the past two decades in ecological theory and  
93 observations (Bustamante et al., 2015; Strigul et al., 2008; Hurtt et al., 1998; Moorcroft et al., 2001)  
94 has made it feasible to include vegetation demography more directly into Earth system models  
95 through individual to cohort-based vegetation in land models (Sato et al., 2007; Watanabe et al.,  
96 2011; Smith et al., 2001; Smith et al., 2014; Weng et al., 2015; Roy et al., 2003; Hurtt et al.,  
97 1998; Fisher et al., 2015). These vegetation demography modules are relatively new in land  
98 models, so tremendous efforts are still under way to improve their parameterizations of resource  
99 competition for light, water, and nutrients, recruitment, mortality, and disturbance including both  
100 natural and anthropogenic components (Fisher et al., 2017).

101 In this study, we aim to (1) describe the development of a selective logging module  
102 implemented into The Functionally Assembled Terrestrial Ecosystem Simulator (FATES), for  
103 simulating anthropogenic disturbances of various intensities to forest ecosystems and their short-  
104 term and long-term effects on water, energy, and carbon cycling, and ecosystem dynamics; (2)  
105 assess the capability of FATES in simulating site-level water, energy, and carbon budgets, as well  
106 as forest structure and composition; (3) benchmark the simulated variables against available  
107 observations at the Tapajós National Forest in the Amazon, thus identifying potential directions  
108 for model improvement; and (4) assess the recovery trajectory of tropical forest following  
109 disturbance under various logging scenarios. In section 2, we provide a brief summary on FATES,  
110 introduce the new selective logging module, and describe numerical experiments performed at two  
111 sites with data from field survey and flux towers. In section 3, FATES-simulated water, energy,



112 and carbon fluxes and stocks in intact and disturbed forests are compared to available observations,  
113 and the effects of logging practice and intensity on forest recovery trajectory in terms of carbon  
114 budget, size structure and composition in plant functional types are assessed. Conclusions and  
115 future work are discussed in section 4.

## 116 **2 Model description and study site**

### 117 **2.1 The Functionally Assembled Terrestrial Ecosystem Simulator**

118 The Functionally Assembled Terrestrial Ecosystem Simulator (FATES) has been developed as a  
119 numerical terrestrial ecosystem model based on the ecosystem demography representation in the  
120 community land model (CLM), formerly known as CLM (ED) (*Fisher et al.*, 2015). FATES is an  
121 implementation of the cohort-based Ecosystem Demography (ED) concept (*Hurtt et al.*,  
122 1998; *Moorcroft et al.*, 2001) that can be called as a library from an ESM land surface scheme,  
123 currently including CLM (*Oleson et al.*, 2013) or Energy Exascale Earth system model (E3SM)  
124 land model (ELM) ([https://climatemodeling.science.energy.gov/projects/energy-exascale-earth-](https://climatemodeling.science.energy.gov/projects/energy-exascale-earth-system-model)  
125 [system-model](https://climatemodeling.science.energy.gov/projects/energy-exascale-earth-system-model)). In FATES, the landscape is discretized into spatially implicit *patches* each of  
126 which represents land areas with a similar *age since last disturbance*. The discretization of  
127 ecosystems along a disturbance/recovery axis allows the deterministic simulation of successional  
128 dynamics within a typical forest ecosystem. Within each patch, individuals are grouped into  
129 *cohorts* by plant functional types (PFTs) and size classes (SCs), so that cohorts can compete for  
130 light based on their heights and canopy positions. Following disturbance, a patch fission process  
131 splits the original patch into undisturbed and disturbed new patches. A patch fusion mechanism is  
132 implemented to merge patches with similar structures, which helps prevent the number of patches  
133 from growing too big. In addition to the ED concept, FATES also adopted a modified version of  
134 the Perfect Plasticity Approximation (PPA) (*Strigul et al.*, 2008) concept by splitting growing  
135 cohorts between canopy and understory layers as a continuous function of height designed for  
136 increasing the probability of co-existence (*Fisher et al.*, 2010). An earlier version of FATES,  
137 CLM(ED), has been applied regionally to explore the sensitivity of biome boundaries to plant trait  
138 representation (*Fisher et al.*, 2015).

139 In this study, we specified two plant functional types (PFTs) in FATES corresponding to  
140 early successional and late successional plants, representative of the primary axis of variability in



141 tropical forests (*Reich* 2014). The early successional PFT is light-demanding, and grows rapidly  
142 under high light conditions common prior to canopy closure. This PFT has low density woody  
143 tissues, shorter leaf and root lifetimes, and a higher background mortality compared to the late  
144 successional PFT that has dense woody tissues, longer leaf and root lifetimes, and lower  
145 background mortality (*Brokaw*, 1985; *Whitmore*, 1998) and thus can survive under deep shade and  
146 grow slowly under closed canopy.

147 The key parameters that differentiate the two PFTs in FATES are listed in Table 1, including  
148 specific leaf area at the canopy top ( $SLA_0$ ), the maximum rate of carboxylation at 25 °C ( $V_{cmax25}$ ),  
149 specific wood density, background mortality, leaf and fine root longevity, and leaf C:N ratio. The  
150 parameter ranges were selected based on literature for tropical forests. Specifically, it has been  
151 reported that  $SLA$  values ranges from 0.007-0.039 m<sup>2</sup> gC<sup>-1</sup> (*Wright et al.*, 2004),  $V_{cmax25}$  ranges  
152 between 10.1 and 105.7 μmol m<sup>-2</sup> s<sup>-1</sup> (*Domingues et al.*, 2005), Specific wood density and  
153 background mortality were set to be 0.5 and 0.9 g cm<sup>3</sup> for early and late succession PFTs,  
154 consistent with those used in the Ecosystem Demography Model version 2 for Amazon forests  
155 (*Longo et al.*, in review) . For simplicity, leaf longevity and root longevity were set to be the same  
156 for each PFT (i.e., 0.9 yr and 2.6 yr for early and late successional PFTs) following the range in  
157 *Trumbore and Barbosa De Camargo* (2009).

158 Given that both  $SLA_0$  and  $V_{cmax25}$  span wide ranges, and have been identified as the most  
159 sensitive parameters in FATES in a previous study (*Massoud et al.*, 2019), we performed one-at-  
160 a-time sensitivity tests by perturbing them within the reported ranges. Based on these tests, it is  
161 evident that these parameters not only affect water, energy, carbon budget simulations, but also  
162 the coexistence of the two PFTs. In the current version of FATES, co-existence of PFTs is not  
163 assured for all parameter combinations, even if they are both within reasonable ranges, on account  
164 of competitive exclusion feedback processes that prevent co-existence in the presence of large  
165 discrepancies in plant growth and reproduction rates (*Fisher et al.* 2010; *Bohn et al.* 2011). In  
166 order to demonstrate FATES' capability in simulating water, energy, carbon budgets as well as  
167 forest structure and composition in a holistic way, we chose to report results based on a set of  
168 parameter values that produces reasonable, stable fractions of two PFTs, as reported in Table 1.

169



## 170 2.2 The selective logging module

171 The new selective logging module in FATES mimics the ecological, biophysical, and  
172 biogeochemical processes following a logging event. The module (1) specifies the timing and  
173 areal extent of a logging event; (2) calculates the fractions of trees that are damaged by direct  
174 felling, collateral damage, and infrastructure damage, and adds these size-specific plant mortality  
175 types to FATES; (3) splits the logged patch into disturbed and intact new patches; (4) applies the  
176 calculated survivorship to cohorts in the disturbed patch; and (5) transports harvested logs off-site  
177 by adding the remaining necromass from damaged trees into coarse woody debris and litter pools.

178 The logging module structure and parameterization is based on detailed field and remote  
179 sensing studies (*Putz et al., 2008; Asner et al., 2004; Pereira Jr et al., 2002; Asner et al.,*  
180 *2005; Feldpausch et al., 2005*). Logging infrastructure including roads, skids, trails, and log decks  
181 are represented (Figure 1). The construction of log decks used to store logs prior to road transport  
182 leads to large canopy openings but their contribution to landscape-level gap dynamics is small. In  
183 contrast, the canopy gaps caused by tree felling are small but their coverage is spatially extensive  
184 at the landscape scale. Variations in logging practices significantly affect the level of disturbance  
185 to tropical forest following logging (*Pereira Jr et al., 2002; Macpherson et al., 2012; Dykstra,*  
186 *2002; Putz et al., 2008*). Logging operations in the tropics are often carried out with little planning,  
187 and typically use heavy machinery to access the forests accompanied by construction of excessive  
188 roads and skid trails, leading to unnecessary tree fall and compaction of the soil. We refer to these  
189 typical operations as conventional logging (CL). In contrast, reduced impact logging (RIL) is a  
190 practice with extensive pre-harvest planning, where trees are inventoried and mapped out for the  
191 most efficient and cost-effective harvest and *seed trees* are deliberately left on site to facilitate  
192 faster recovery. Through planning, the construction of skid trails and roads, soil compaction and  
193 disturbance can be minimized. Vines connecting trees are cut and tree-fall directions are  
194 controlled to reduce damages to surrounding trees. Reduced impact logging results in consistently  
195 less disturbance to forests than conventional logging (*Pereira Jr et al. 2002; Putz et al. 2008*).

196 The FATES logging module was designed to represent a range of logging practices in field  
197 operations at a landscape level. Once logging events are activated, we define three types of  
198 mortality associated with logging practices: direct-felling mortality ( $l_{\text{mort}_{\text{direct}}}$ ), collateral  
199 mortality ( $l_{\text{mort}_{\text{collateral}}}$ ), and mechanical mortality ( $l_{\text{mort}_{\text{mechanical}}}$ ). The direct felling mortality  
200 represents the fraction of trees selected for harvesting that are greater or equal to a diameter





201 threshold (this threshold is defined by the diameter at breast height (DBH) = 1.3 m denoted as  
202  $DBH_{min}$ ); collateral mortality denotes the fraction of adjacent trees that killed by felling of the  
203 harvested trees; and the mechanical mortality represents the fraction of trees killed by construction  
204 of log decks, skid trails and roads for accessing the harvested trees, as well as storing and  
205 transporting logs offsite (Figure 1a). In a logging operation, the loggers typically avoid large trees  
206 when they build log decks, skids, and trails by knocking down relatively small trees as it is not  
207 economical to knock down large trees. Therefore, we implemented another DBH threshold,  
208  $DBH_{max\_infra}$ , so that only a fraction of trees  $\leq DBH_{max\_infra}$  (called mechanical damage fraction)  
209 are removed for building infrastructure (Feldpausch *et al.*, 2005).

210 To capture the disturbance mechanisms and degree of damage associated with logging  
211 practices at the landscape level, we apply the mortality types following a workflow designed to  
212 correspond to field operations. In FATES, as illustrated in Figure 2, individual trees of all plant  
213 functional types (PFTs) in one patch are grouped into cohorts of similar-sized trees, whose size  
214 and population sizes evolve in time through processes of recruitment, growth, and mortality. For  
215 the purpose of reporting and visualizing the model state, these cohorts are binned into a set of 13  
216 fixed size classes in terms of the diameter at the breast height (DBH) (i.e., 0 – 5, 5 – 10, 10 – 15,  
217 15 – 20, 20 – 30, 30 – 40, 40 – 50, 50 – 60, 60 – 70, 70 – 80, 80 – 90, 90 – 100, and  $\geq 100$  cm).  
218 Cohorts are further organized into canopy and understory layers, which are subject to different  
219 light conditions (Figure 2a). When logging activities occur, the canopy trees and a portion of big  
220 understory trees lose their crown coverage through direct felling for harvesting logs, or as a result  
221 of collateral and mechanical damages (Figure 2b). The fractions of (only the) canopy trees affected  
222 by the three mortality mechanisms are then summed up to specify the areal percentages of an old  
223 (undisturbed) and a new (disturbed) patch caused by logging in the patch fission process as  
224 discussed section 2.1 (Figure 2c). After patch fission, the canopy layer over the disturbed patch  
225 is removed, while that over the undisturbed patch stays untouched (Figure 2d). In the undisturbed  
226 patch, the survivorship of understory trees is calculated using an understory death fraction  
227 consistent with whose default value corresponds to that used for natural disturbance (i.e., 0.5598).  
228 To differentiate logging from natural disturbance, a slightly elevated, logging-specific understory  
229 death fraction is applied in the disturbed patch instead at the time of the logging event. Based on  
230 data from field surveys over logged forest plots in southern Amazon (Feldpausch *et al.*, 2005),  
231 understory death fraction corresponding to logging is now set to be 0.65 as the default, but can be





232 modified via the FATES parameter file (Figure 2e). Therefore, the logging operations will change  
 233 the forest from the undisturbed state shown in Figure 2a to a disturbed state in Figure 2f in the  
 234 logging module. It is worth mentioning that the newly generated patches are tracked according to  
 235 *age since disturbance* and will be merged with other patches of similar canopy structure following  
 236 the patch fusion processes in FATES in later time steps of a simulation, pending the inclusion of  
 237 separate land-use fractions for managed and unmanaged forest.

238 Logging operations affect forest structure and composition, and also carbon cycling (*Palace et al.*  
 239 *et al.*, 2008) by modifying the live biomass pools and flow of necromass (Figure 3). Following a  
 240 logging event, the logged trunk products from the harvested trees are transported off-site (as an  
 241 added carbon pool for resource management in the model), while their branches enter the coarse  
 242 woody debris (CWD) pool, and their leaves and fine roots enter the litter pool. Similarly, trunks  
 243 and branches of the dead trees caused by collateral and mechanical damages also become CWD,  
 244 while their leaves and fine roots become litter. Specifically, the densities of dead trees as a result  
 245 of direct felling, collateral, and mechanical damages in a cohort are calculated as follows:

$$\begin{aligned}
 D_{\text{direct}} &= \text{lmort}_{\text{direct}} \times \frac{n}{A} \\
 D_{\text{collateral}} &= \text{lmort}_{\text{collateral}} \times \frac{n}{A} \\
 D_{\text{mechanical}} &= \text{lmort}_{\text{mechanical}} \times \frac{n}{A}
 \end{aligned}
 \tag{1}$$

247 where  $A$  stands for the area of the patch being logged, and  $n$  is the number of individuals in the  
 248 cohort where the mortality types apply (i.e., as specified by the size thresholds,  $\text{DBH}_{\text{min}}$  and  
 249  $\text{DBH}_{\text{max\_infra}}$ ). For each cohort, we denote  $D_{\text{indirect}} = D_{\text{collateral}} + D_{\text{mechanical}}$  and  $D_{\text{total}} =$   
 250  $D_{\text{direct}} + D_{\text{indirect}}$ , respectively.

251 Leaf litter ( $\text{Litter}_{\text{leaf}}$ , [kg C]) and root litter ( $\text{Litter}_{\text{root}}$ , [kg C]) at the cohort level are then  
 252 calculated as:

$$\text{Litter}_{\text{leaf}} = D_{\text{total}} \times B_{\text{leaf}} \times A
 \tag{2}$$

$$\text{Litter}_{\text{root}} = D_{\text{total}} \times (B_{\text{root}} + B_{\text{store}}) \times A
 \tag{3}$$

255 where  $B_{\text{leaf}}$ ,  $B_{\text{root}}$ , and  $B_{\text{store}}$  are live biomass in leaves and fine roots, and stored biomass in  
 256 the labile carbon reserve in all individual trees in the cohort of interest.

257 Following the existing CWD structure in FATES (*Fisher et al.*, 2015), CWD in the logging  
 258 module is first separated into two categories: above-ground CWD and below-ground CWD.



259 Within each category, four size classes are tracked based on their source, following Thonicke et  
 260 al. (2010): trunks, large branches, small branches and twigs. Above-ground CWD from trunks  
 261 ( $CWD_{\text{trunk\_agb}}$ , [kg C]) and large branches/small branches/twig ( $CWD_{\text{branch\_agb}}$ , [kg C]) are  
 262 calculated as follows:

$$263 \quad CWD_{\text{trunk\_agb}} = D_{\text{indirect}} \times B_{\text{stem\_agb}} \times f_{\text{trunk}} \times A \quad (4)$$

$$264 \quad CWD_{\text{branch\_agb}} = D_{\text{total}} \times B_{\text{stem\_agb}} \times f_{\text{branch}} \times A \quad (5)$$

265 where  $B_{\text{stem\_agb}}$  is the amount of above ground stem biomass in the cohort,  $f_{\text{trunk}}$  and  $f_{\text{branch}}$   
 266 represent the fraction of trunks and large branches/small branches/twig. Similarly, the below-  
 267 ground CWD from trunks ( $CWD_{\text{trunk\_bg}}$ , [kg C]) and branches/twig ( $CWD_{\text{branch\_bg}}$ , [kg C]) are  
 268 calculated as follows:

$$269 \quad CWD_{\text{trunk\_bg}} = D_{\text{total}} \times B_{\text{root\_bg}} \times f_{\text{trunk}} \times A \quad (6)$$

$$270 \quad CWD_{\text{branch\_bg}} = D_{\text{total}} \times B_{\text{root\_bg}} \times f_{\text{branch}} \times A \quad (7)$$

271 where  $B_{\text{root}}$  [kg C] is the amount of coarse root biomass in the cohort. Site-level total litter and  
 272 CWD inputs can then be obtained by integrating the corresponding pools over all the cohorts in  
 273 the site. To ensure mass conservation,

$$274 \quad \Delta B = \Delta \text{Litter} + \Delta \text{CWD} + \text{trunk\_product} \quad (8)$$

275 where  $\Delta B$  is total loss of biomass due to logging,  $\Delta \text{Litter}$  and  $\Delta \text{CWD}$  are the increments in litter  
 276 and CWD pools, and *trunk\_product* represents harvested logs shipped offsite.

277 Following the logging event, the forest structure and composition in terms of cohort  
 278 distributions, as well as the live biomass and necromass pools are updated. Following this logging  
 279 event update to forest structure, the native processes simulating physiology, growth and  
 280 competition for resources in and between cohorts resume. Since the canopy layer is removed in  
 281 the disturbed patch, the existing understory trees are promoted to the canopy layer, but, in general,  
 282 the canopy is incompletely filled in by these newly-promoted trees, and thus the canopy does not  
 283 fully close. Therefore, more light can penetrate and reach the understory layer in the disturbed  
 284 patch, leading to increases in light-demanding species in the early stage of regeneration, followed  
 285 by a succession process in which shade tolerant species dominate gradually.

286



### 287 2.3 Study site and data

288 In this study, we used data from two evergreen tropical forest sites located in the Tapajós National  
289 Forest (TNF), Brazil (Figure 1b). These sites were established during the Large-Scale Biosphere-  
290 Atmosphere Experiment in Amazonia (LBA), and are selected because of data availability  
291 including those from forest plot surveys and two flux towers established during the LBA period  
292 (*Keller et al.*, 2004a). These sites were named after distances along the BR-163 highway from  
293 Santarém: km67 (54°58'W, 2°51'S) and km83 (54°56'W, 3°3'S). They are situated on a flat  
294 plateau and were established as a control-treatment pair for a selective logging experiment. Tree  
295 felling operations were initiated at km83 in September 2001 for a period of about two months.  
296 Both sites are similar with mean annual precipitation of ~2000 mm, and mean annual temperature  
297 of 25 °C, on nutrient-poor clay oxisols with low organic content (*Silver et al.*, 2000).

298 Prior to logging, both sites were old-growth forests with limited previous human disturbances  
299 caused by hunting, gathering Brazil nuts, and similar activities. A comprehensive set of  
300 meteorological variables, as well as land-atmosphere exchanges of water, energy, and carbon  
301 fluxes have been measured by an eddy covariance tower at a hourly time step over the period of  
302 2002 to 2011, including precipitation, air temperature, surface pressure, relative humidity,  
303 incoming shortwave and longwave radiation, latent and sensible heat fluxes, and net ecosystem  
304 exchange (NEE) (*Hayek et al.*, 2018). Another flux tower was established at km83, the logged  
305 site, with hourly meteorological and eddy covariance measurements in the period of 2000-2003  
306 (*Miller et al.*, 2004; *Goulden et al.*, 2004; *Saleska et al.*, 2003). The towers are listed as BR-Sa1  
307 and BR-Sa3 in the AmeriFlux network (<https://ameriflux.lbl.gov>).

308 These tower and biometric based observations were summarized to quantify logging-induced  
309 perturbations on old-growth Amazonian forests in *Miller et al.* (2011) and are used in this study to  
310 benchmark the model simulated carbon budget. Over the period of 1999 to 2001, all trees  $\geq 35$ cm  
311 in DBH in 20 ha of forest in four 1-km long transects within the km67 footprint were inventoried,  
312 as well as trees  $\geq 10$  cm in DBH on subplots with an area of ~4 ha. At km83, inventory surveys on  
313 trees  $\geq 55$  cm in DBH were conducted in 1984 and 2000, and another survey on trees  $> 10$  cm in  
314 DBH was conducted in 2000 (*Miller et al.*, 2004). Estimates of above ground biomass (AGB) were  
315 then derived using allometric equation for Amazon forests (*Rice et al.*, 2004; *Chambers et al.*,  
316 2004; *Keller et al.*, 2001). Necromass ( $\geq 2$  cm diameter) production was also measured  
317 approximately every six months in a 4.5-year period from November 2001 through February 2006



318 in logged and undisturbed forest at km83 (*Palace et al.*, 2008). Field measurements of ground  
319 disturbance in terms of number of felled trees, areas disturbed by collateral and mechanical  
320 damages were also conducted at a similar site in Pará state along multitemporal sequences of post-  
321 harvest regrowth of 0.5–3.5 yr (*Asner et al.*, 2004; *Pereira Jr et al.*, 2002).

322 Table 2 provides a summary of stem density and basal area distribution across size classes at  
323 km83 based on the biomass survey data (*Menton et al.* 2011; *de Sousa et al.*, 2011). To facilitate  
324 comparisons with simulations from FATES, we divided the inventory into early and late  
325 succession PFTs using threshold of  $0.7 \text{ g cm}^{-3}$  for specific wood density, consistent with the  
326 definition of these PFTs in Table 1. As shown in Table 2, prior to the logging event in year 2000,  
327 this forest was composed of 399, 30 & 30 trees per hectare in size classes of 10-30 cm, 30-50 cm,  
328 and  $\geq 50$  cm respectively; Following logging, the numbers were reduced to 396, 29, and 18 trees  
329 per hectare, losing  $\sim 1.3\%$  of trees  $\geq 10$  cm in size. The changes in stem density (SD) were caused  
330 by different mechanisms for different size classes. The reduction in stem density of  $2 \text{ ha}^{-1}$  in the  
331  $\geq 50$  cm size class was caused by timber harvest directly, while the reductions of  $3 \text{ ha}^{-1}$  and  $1 \text{ ha}^{-1}$   
332 in the 10-30 cm and 30-50 cm size classes were caused by collateral and mechanical damages.  
333 Corresponding to the loss of trees in logging operations, basal area (BA) decreased from 3.9, 4.0,  
334 and  $12.9 \text{ m}^2 \text{ ha}^{-1}$  to 3.8, 3.9, and  $10.8 \text{ m}^2 \text{ ha}^{-1}$ , and above ground biomass (AGB) decreased from  
335 3.8, 2.3, and  $10.4 \text{ kg C m}^{-2}$  to 3.8, 2.2,  $8.7 \text{ kg C m}^{-2}$  in the 10-30 cm, 30-50 cm, and  $\geq 50$  cm size  
336 class, respectively.

## 337 2.4 Numerical Experiments

338 In this study, the gap-filled meteorological forcing data for Tapajós National Forest processed by  
339 *Longo* (2014) are used to drive the CLM(FATES) model. Characteristics of the sites, including  
340 soil texture, vegetation cover fraction, and canopy height, were obtained from the LBA-Data  
341 Model Intercomparison Project (*de Gonçalves et al.*, 2013). Specifically, soil at km 67 contains  
342 90% clay and 2% sand, while soil at km 83 contains 80% clay and 18% sand. Both sites are covered  
343 by tropical evergreen forest at  $\sim 98\%$  within their footprints, with the remaining 2% assumed to  
344 be covered by bare soil. As discussed in *Longo et al.* (2018), who deployed the Ecosystem  
345 Demography model version 2 at this site, soil texture and hence soil hydraulic parameters are  
346 highly variable even with the footprint of the same eddy covariance tower, and could have  
347 significant impacts on not only water and energy simulations, but also simulated forest



348 composition and carbon stocks and fluxes. Further, generic pedo-transfer functions designed to  
349 capture temperate soils typically perform poorly in clay-rich Amazonian soils (*Fisher et al.* 2008,  
350 *Tomasella and Hodnett*, 1998). Because we focus on introducing the FATES-logging, we leave  
351 for forthcoming studies the exploration of the sensitivity of the simulations to soil texture and other  
352 critical environmental factors.

353 CLM(FATES) was initialized using soil texture at km83 (i.e., 80% clay and 18% sand) from  
354 bare ground and spun up for 800 years until the carbon pools and forest structure (i.e., size  
355 distribution) and composition of PFTs reached equilibrium, by recycling the meteorological  
356 forcing at km67 (2001-2011) as the sites are close enough. The final states from spin-up were  
357 saved as the initial condition for follow-up simulations. An *intact* experiment was conducted by  
358 running the model over a period of 2001 to 2100 without logging by recycling the 2001-2011  
359 forcing using the parameter set in Table 1. The atmospheric CO<sub>2</sub> concentration was assumed to be  
360 a constant of 367 ppm over the entire simulation period, consistent with the CO<sub>2</sub> levels during the  
361 logging treatment (*Dlugokencky et al.*, 2017).

362 We specified an experimental logging event in FATES on 1 September 2001 (Table 3). It  
363 was reported by *Figueira et al.* (2008) that following the reduced impact logging event in  
364 September 2001, 9% of the trees greater or equal to  $DBH_{min} = 50$  cm were harvested, with an  
365 associated collateral damage fraction of 0.009 for trees  $\geq DBH_{min}$ .  $DBH_{max\_infra}$  is set to be 30 cm,  
366 so that only a fraction of trees  $\leq 30$  cm are removed for building infrastructure (*Feldpausch et al.*,  
367 2005). This experiment is denoted as the  $RIL_{low}$  experiment in Table 2 and is the one that matches  
368 the actual logging practice at km83.

369 We recognize that the harvest intensity in September 2001 at km83 was extremely low.  
370 Therefore, in order to study the impacts of different logging practices and harvest intensities, three  
371 additional logging experiments were conducted as listed in Table 3: conventional logging with  
372 high intensity ( $CL_{high}$ ), conventional logging with low intensity ( $CL_{low}$ ), and reduced impact  
373 logging with high intensity ( $RIL_{high}$ ). The high intensity logging doubled the direct felling fraction  
374 in  $RIL_{low}$  and  $CL_{low}$ , as shown in the  $RIL_{high}$  and  $CL_{high}$  experiments. Compared to the  $RIL$   
375 experiments, the  $CL$  experiments feature elevated collateral and mechanical damages as one would  
376 observe in such operations. All logging experiments were initialized from the spun-up state using  
377 site characteristics at km83 previously discussed and were conducted over the period of 2001-2100  
378 by recycling meteorological forcing from 2001- 2011.



### 379 3 Results and discussions

#### 380 3.1 Simulated energy and water fluxes

381 Simulated monthly mean energy and water fluxes at the two sites are shown and compared to  
382 available observations in Figure 4. The performances of the simulations closest to site conditions  
383 were compared to observations and summarized in Table 4 (i.e., intact for km67 and RIL<sub>low</sub> for  
384 km83). The observed fluxes as well as their uncertainty ranges noted as Obs67 and Obs83 from  
385 the towers were obtained from *Saleska et al. (2013)*, consistent with those in *Miller et al. (2011)*.  
386 As shown in Table 4, the simulated mean ( $\pm$ standard deviation) latent heat (LH), sensible heat  
387 (SH), and net radiation (Rn) fluxes at km83 in RIL<sub>low</sub> over the period of 2001-2003 are  $108.3 \pm$   
388  $20.8$ ,  $20.5 \pm 24.3$  and  $128.9 \pm 15.5$  W m<sup>-2</sup>, compared to tower-based observations of  $101.6 \pm 8.0$ ,  
389  $25.6 \pm 5.2$  and  $129.3 \pm 18.5$  W m<sup>-2</sup>. Therefore, the simulated and observed Bowen ratios are 0.16  
390 and 0.20 at km83, respectively. This result suggests that at an annual time step, the observed  
391 partitioning between LH and SH are reasonable. However, at seasonal scales, even though net  
392 radiation is captured by CLM (FATES), the model does not adequately partition sensible and latent  
393 heat fluxes. This is particularly true for sensible heat fluxes as the model simulates large seasonal  
394 variabilities in SH when compared to observations at the site (i.e., standard deviations of monthly-  
395 mean simulated SH are  $\sim 24.3$  W m<sup>-2</sup>, while observations are  $\sim 5.2$  W m<sup>-2</sup>). As illustrated in figures  
396 4(c) and 4(d), the model significantly overestimates SH in the dry season (June-December), while  
397 it slightly underestimates SH in the wet season. It is worth mentioning that incomplete closure of  
398 the energy budget is common at eddy covariance towers (*Wilson et al., 2002; Foken, 2008*) and has  
399 been reported to be  $\sim 87\%$  at the two sites (*Saleska et al., 2003*). Nevertheless, some of the  
400 mismatches between observations and simulations can be attributed to structural problems in this  
401 version of FATES. For example, the mean simulated leaf area indices (LAIs) are  $\sim 2.4$  m<sup>2</sup>m<sup>-2</sup>, while  
402 observations suggest that LAIs at these sites ranges from 5-7 m<sup>2</sup>m<sup>-2</sup> (*Doughty and Goulden,*  
403 *2008; Brando et al., 2010*). The low LAI bias in the model leads to lower simulated LH, and in  
404 turn the overestimation of SH to conserve energy.

405 Figure 4(j) shows the comparison between simulated and observed (*Goulden et al., 2010*)  
406 volumetric soil moisture content (m<sup>3</sup>m<sup>-3</sup>) at top 10 cm. This comparison reveals another model  
407 structural deficiency, that is, even though the model simulates higher soil moisture contents  
408 compared to observations (a feature generally attributable to the soil moisture retention curve), the  
409 transpiration beta factor, the down-regulating factor of transpiration from plants, fluctuates



410 significantly over a wide range, and can be as low as 0.13 in the dry season. In reality flux towers  
411 in the Amazon generally do not show severe moisture limitations in the dry season (*Fisher et al.*  
412 2007). The lack of limitation is typically attributed to the plant's ability to extract soil moisture  
413 from deep soil layers, a phenomenon that is difficult to simulate using a classical beta function  
414 (*Baker et al.* 2008), and potentially is reconcilable using hydrodynamic representation of plant  
415 water uptake (*Powell et al.* 2014; *Christoffersen et al.* 2016) as are in the final stages of  
416 incorporation into the FATES model. Consequently, the model simulates consistently low ET  
417 during dry seasons (figures 4(e) and 4(f)), while observations indicate that canopies are highly  
418 productive owing to adequate water supply to support transpiration and photosynthesis, which  
419 could further stimulate coordinated leaf growth with senescence during the dry season (*Wu et al.*  
420 2016; 2017).

421

### 422 **3.2 Carbon budget, and forest structure and composition in the intact forest**

423 Figures 5, 6, and 7 show simulated carbon pools and fluxes, which are tabulated in Table 5 as well.  
424 As shown in Figure 5, prior to logging, the simulated above ground biomass and necromass (CWD  
425 + litter) are 155 Mg C ha<sup>-1</sup> and 41.1 Mg C ha<sup>-1</sup>, compared to 165 Mg C ha<sup>-1</sup> and 58.4 Mg C ha<sup>-1</sup>  
426 based on permanent plot measurements. The simulated carbon pools are generally lower than  
427 observations reported in *Miller et al.* (2011) but are within reasonable ranges, as errors associated  
428 with these estimates could be as high as 50% due to issues related to sampling and allometric  
429 equations, as discussed in *Keller et al.* (2001). The lower biomass estimates are consistent with the  
430 finding of excessive soil moisture stress during the dry season, and low LAI in the model.

431 Combining forest inventory and eddy covariance measurements, *Miller et al.* (2011) also  
432 provides estimates for net ecosystem exchange (NEE), gross primary production (GPP), net  
433 primary production (NPP), ecosystem respiration (ER), heterotrophic respiration (HR), and  
434 autotrophic respiration (AR). As shown in Table 5, the model simulates a NPP of 8.9 Mg C ha<sup>-2</sup>  
435 yr<sup>-1</sup> and a HR of 9.4 Mg C ha<sup>-2</sup> yr<sup>-1</sup>, in comparison to the estimated NPP of 9.5 Mg C ha<sup>-2</sup> yr<sup>-1</sup> and  
436 HR of 8.9 Mg C ha<sup>-2</sup> yr<sup>-1</sup> in the intact forest based on field measurements. This suggests that despite  
437 the low LAI, the model nonetheless captures the turnover of the live carbon pools and the decay  
438 rates of the necromass pools reasonably well. However, the model simulates much lower values  
439 in GPP (17.6 Mg C ha<sup>-2</sup> yr<sup>-1</sup>), AR (8.7 Mg C ha<sup>-2</sup> yr<sup>-1</sup>), and ER (18.1 Mg C ha<sup>-2</sup> yr<sup>-1</sup>), when  
440 compared to values estimated from the observations (32.6 Mg C ha<sup>-2</sup> yr<sup>-1</sup> for GPP, 23.1 Mg C ha<sup>-2</sup>





441  $\text{yr}^{-1}$  for AR, and  $31.9 \text{ Mg C ha}^{-2} \text{ yr}^{-1}$  for ER). The low biases in simulated AGB, GPP, AR and  
442 leaf area index (figures 4g and 4h) suggests that this version of the model suffers from parametric  
443 uncertainties in its capability of establishing enough live plant tissues for photosynthesis and  
444 autotrophic respiration at the patch level that are the subject of ongoing updates and modifications.  
445 Compensating errors in the gross fluxes, however, produce reasonable NPP estimates, making all  
446 the ecosystem processes downstream of NPP within the observed ranges.

447 Consistent with the carbon budget terms, Table 5 lists the simulated and observed values of  
448 stem density ( $\text{ha}^{-1}$ ) in different size classes in term of DBH. The model simulates 232 trees per  
449 hectare with DBHs greater than or equal to 10 cm in the intact forest, compared to 459 trees per  
450 hectare from observed inventory. In terms of distribution across the DBH classes of 10-30 cm, 30-  
451 50 cm, and  $\geq 50$  cm, 145, 43, and 44  $\text{N ha}^{-1}$  of trees were simulated, while 399, 30, and 30  $\text{N ha}^{-1}$   
452 were observed in the intact forest. In general, this version of FATES is simulating a less dense  
453 forest, with a forest structure biased toward larger trees, a feature that may result from allometric  
454 considerations. Trees have a maximum crown area in FATES, after which DBH increases but  
455 spatial extent does not. If this crown-area threshold is too high, a limited number of crowns will  
456 fit into the canopy, leading to low biases in number density. In addition to size distribution, by  
457 parametrizing early and late successional PFTs (Table 1), FATES is capable of simulating the co-  
458 existence of the two PFTs, therefore the PFT-specific trajectories of stem density, basal area,  
459 canopy and understory mortality rates. We will discuss these in section 3.4.

460

461

### 462 **3.3 Effects of logging on water, energy, and carbon budgets**

463 The response of energy and water budgets to different levels of logging disturbances are illustrated  
464 in Table 4 and Figure 4. Following the logging event, the LAI is reduced proportionally to the  
465 logging intensities (-7%, -15%, -9% and -17% for  $\text{RL}_{\text{low}}$ ,  $\text{RL}_{\text{high}}$ ,  $\text{CL}_{\text{low}}$ , and  $\text{CL}_{\text{high}}$  respectively  
466 in September 2001, see figure 4h). Leaf area index recovers within three years to its pre-logging  
467 level, or even to slightly higher levels as a result of the improved light environment following  
468 logging leading to changes in forest structure and composition (to be discussed in section 3.4). In  
469 response to the changes in stem density and LAI, discernible differences are found in all energy  
470 budget terms. For example, less leaf area leads to reductions in LH (-0.5%, -1.0%, -6.9%, -7.4%)  
471 and increases in SH (4.0%, 8.0%, 4.4%, and 8.6%) proportional to the damage levels (i.e.,  $\text{RL}_{\text{low}}$ ,



472  $RL_{high}$ ,  $CL_{low}$ , and  $CL_{high}$ ) in the first three years following the logging event when compared to  
473 the control simulation. Energy budget responses scale with the level of damage, so that the biggest  
474 differences are detected in the  $CL_{high}$  scenario, followed by  $RIL_{high}$ ,  $CL_{low}$  and  $RIL_{low}$ . The  
475 difference in simulated water and energy fluxes between the  $RIL_{low}$  (i.e., the scenario that is the  
476 closest to the experimental logging event) and intact cases is the smallest, as the level of damage  
477 is the lowest among all scenarios.

478 As with LAI, the water and energy fluxes recover rapidly in 3-4 years following logging.  
479 *Miller et al.* (2011) compared observed sensible and latent heat fluxes between the control (km67)  
480 and logged sites (km83). They found that in the first three years following logging, the between-  
481 sites difference (i.e., logged – control) in LH reduced from  $19.7 \pm 2.4$  to  $15.7 \pm 1.0$  W m<sup>2</sup>, and that  
482 in SH increased from  $3.6 \pm 1.1$  to  $5.4 \pm 0.4$  W m<sup>2</sup>. When normalized by observed fluxes during the  
483 same periods at km83, these changes correspond to a -4% reduction in LH and a 7% increase in  
484 SH, compared to the -0.5% and 4% differences in LH and SH between  $RL_{low}$  and the control  
485 simulations. In general, both observations and our modelling results suggest that the impacts of  
486 reduced impact logging on energy fluxes are modest and that the energy and water fluxes can  
487 quickly recover to their pre-logging conditions at the site.

488 Figures 6 and 7 show the impact of logging on carbon fluxes and pools at a monthly time  
489 step, and the corresponding annual fluxes and changes in carbon pools are summarized in Table 5.  
490 The logging disturbance leads to reductions in GPP, NPP, AR, and AGB, and increases in ER,  
491 NEE, HR, and CWD. The impacts of logging on the carbon budgets are also proportional to  
492 logging damage levels. Specifically, logging reduces the simulated AGB from 155 Mg C ha<sup>-1</sup>  
493 (intact) to 138.0 Mg C ha<sup>-1</sup> ( $RIL_{low}$ ), 119.3 Mg C ha<sup>-1</sup> ( $RIL_{high}$ ), 137.8 Mg C ha<sup>-1</sup> ( $CL_{low}$ ) and 118.9  
494 ( $CL_{high}$ ), while increases the simulated necromass pool (CWD + litter) from 41.1 Mg C ha<sup>-1</sup> in the  
495 intact case to 59.6 Mg C ha<sup>-1</sup> ( $RIL_{low}$ ), 79.5 Mg C ha<sup>-1</sup> ( $RIL_{high}$ ), 60.0 Mg C ha<sup>-1</sup> ( $CL_{low}$ ) and 80.1  
496 ( $CL_{high}$ ). For the case closest to the experimental logging event ( $RIL_{low}$ ), the changes in AGB and  
497 necromass from the intact case are -17 Mg C ha<sup>-1</sup> (11%) and 18.5 Mg C ha<sup>-1</sup> (45%), in comparison  
498 to observed changes of -22 Mg C ha<sup>-1</sup> in AGB (12%) and 16 Mg C ha<sup>-1</sup> (27%) in necromass from  
499 *Miller et al.* (2011), respectively. The negative model biases in carbon pools, GPP, ER, and AR  
500 (see section 3.2) propagate into their estimates following disturbance (Table 5), but the directions  
501 of their changes are reasonable when compared to observations (i.e., decreases in GPP, ER, and  
502 AR following logging). On the other hand, the simulations indicate that the forest could be turned



503 from a small carbon source ( $0.5 \text{ Mg C ha}^{-1} \text{ yr}^{-1}$ ) to a larger carbon source in 1-5 years following  
504 logging, while observations from the tower suggested that the forest was a carbon sink or a modest  
505 carbon source ( $-0.6 \pm 0.8 \text{ Mg C ha}^{-1} \text{ yr}^{-1}$ ) prior to logging, and turned into a carbon sink in three  
506 years following logging. Such a mismatch between observations and simulations is a result of a  
507 less productive forest in the model.

508 The recovery trajectories following logging are also shown in figures 6, 7, and Table 5. It  
509 takes more than 70 years for AGB to return to its pre-logging levels, but the recovery of carbon  
510 fluxes such as GPP, NPP, and AR is much faster (i.e., within five years following logging). The  
511 initial recovery rates of AGB following logging are faster for high-intensity logging because  
512 increased light reaching the forest floor, as indicated by the steeper slopes corresponding to the  
513  $\text{CL}_{\text{high}}$  and  $\text{RIL}_{\text{high}}$  scenarios compared to those of  $\text{CL}_{\text{low}}$  and  $\text{RIL}_{\text{low}}$  (figure 9h). While this finding  
514 is consistent with previous observational and modelling studies (*Mazzei et al.*, 2010; *Huang and*  
515 *Asner*, 2010) in that the damage level determines the number of years required to recover the  
516 original AGB, and the AGB accumulation rates in recently logged forests are higher than that in  
517 intact forest, the simulated recovery time is slower than that reported in literature. For example, by  
518 synthesizing data from 79 permanent plots at 10 sites across the Amazon basin, *Ruttishauser et al.*  
519 (2016) and *Piponiot et al.* (2018) show that it requires 12, 43, and 75 years for the forest to recover  
520 with initial losses of 10, 25, or 50% in AGB. The slow recovery time in the simulation might be  
521 attributed to the low GPP bias in this version of CLM (FATES). Corresponding to the changes  
522 in AGB, logging introduces a large amount of necromass to the forest floor, with the highest  
523 increases in the  $\text{CL}_{\text{high}}$  and  $\text{RIL}_{\text{high}}$  scenarios. As shown in Figure 7(d) and Table 5, necromass and  
524 CWD pools return to the pre-logging level in ~15 years. Meanwhile, HR in  $\text{RIL}_{\text{low}}$  stays elevated  
525 in five years following logging but converges to that from the intact simulation in ~10 years, which  
526 is consistent with observation (*Miller et al.* 2011; Table 5).

527

### 528 **3.4 Effects of logging on forest structure and composition**

529 The capability of the CLM(FATES) model to simulate vegetation demographics, forest structure  
530 and composition, while simulating the water, energy, and carbon budgets simultaneously (Fisher  
531 et al. 2017) allows interrogation of the modelled impacts of alternative logging practices on forest  
532 size structure. Table 6 shows forest structure in terms of stem density distribution across size  
533 classes from the simulations compared to observations from the site, while figures 8 and 9 further



534 break it down into early and late succession PFTs and size classes in terms of stem density and  
535 basal areas. As discussed in section 2.2 and summarized in Table 3, the logging practices, reduced  
536 impact logging and conventional logging, differ in terms of pre-harvest planning and actual field  
537 operation to minimize collateral and mechanical damages, while the logging intensities (i.e., high  
538 and low) indicate the target direct felling fractions. The corresponding outcomes of changes in  
539 forest structure in comparison to the intact forest, as simulated by FATES, are summarized in  
540 tables 6 and 7. The conventional logging scenarios (i.e.,  $CL_{high}$  and  $CL_{low}$ ), feature more losses in  
541 small trees less than 30 cm in DBH, when compared to the smaller reduction in stem density in  
542 size classes less than 30 cm in DBH in the reduced impact logging scenarios (i.e.,  $RIL_{high}$  and  
543  $RIL_{low}$ ). Scenarios with different logging intensities (i.e., high and low) result in different direct  
544 felling intensity. That is, the number of surviving large trees ( $DBH \geq 30$  cm) in  $RIL_{low}$  and  $CL_{low}$   
545 is  $81 \text{ ha}^{-1}$ , but those in  $RIL_{high}$  and  $CL_{high}$  is  $75 \text{ ha}^{-1}$ .

546 In response to the improved light environment after removal of large trees, early successional  
547 trees quickly establish and populate the tree fall gaps following logging in 2-3 years as shown  
548 Figure 8a). Stem density in the  $<10$  cm size classes is proportional to the damage levels (i.e.,  
549 ranked as  $CL_{high} > RIL_{high} > CL_{low} > RIL_{low}$ ), followed by a transition to late successional trees in  
550 later years when the canopy is closed again (Figure 8b). Such a successional process is also evident  
551 in figures 9(a) and 9(b) in terms of basal areas. The number of early successional trees then slowly  
552 declines afterwards but is sustained throughout the simulation as a result of natural disturbances.  
553 Such a shift in the plant community towards light-demanding species following disturbances is  
554 consistent with observations reported in literature (*Baraloto et al.*, 2012; *Both et al.*, 2018).  
555 Following regeneration in logging gaps, a fraction of the late successional trees wins the  
556 competition within the 0-10 cm size classes and is promoted to the 10-30 cm size classes in about  
557 10 years following the disturbances (figures 8d and 9d). Then a fraction of those trees  
558 subsequently enter the 30-50 cm size classes in 20-40 years following the disturbance (figures 8f  
559 and 9f) and so on through larger size classes afterwards (figures 8h and 9h). We note that despite  
560 the goal of achieving a deterministic and smooth averaging across discrete stochastic disturbance  
561 events using the ecosystem demography approach (*Moorcroft et al.*, 2001) in FATES, the  
562 successional process described above, as well as the total numbers of stems in each size bin, shows  
563 evidence of episodic and discrete waves of population change. These arise due to the required



564 discretization of the continuous time-since-disturbance heterogeneity into patches, combined with  
565 the current maximum cap on the number of patches in FATES (10 per site).

566 As discussed in section 2.4, the understory early successional trees have a high mortality  
567 (figure 10a) compared to the mortality (figure 10b) of understory late successional trees because  
568 they are shade intolerant. As a result, early successional trees can barely survive in the understory.  
569 Therefore, mortality for understory early successional trees cannot be calculated due to the lack of  
570 population (figures 10c, e, and g). The mortality of large late successional understory trees  
571 gradually increases as more light and water are needed to sustain the trees as they grow larger  
572 (figures 10d, f), and drops again due to lack of population in the >50cm size class. The mortality  
573 rates of small canopy trees (both early and late, as shown in figures 11a and b) decline in the first  
574 few years following logging, and then fluctuate at an equilibrium level because only small  
575 disturbed patches can be created as a result of natural disturbances after the initial logging event.  
576 Mortality rates of large canopy trees (figures 11c-h) are pretty stable, indicating that canopy trees  
577 are not light-limited or water-stressed. Basal area is generally higher in late successional PFT than  
578 in early successional PFT (figure 9) despite its high stem density.

#### 579 **4 Conclusion and Discussions**

580 In this study, we developed a selective logging module in FATES and parameterized the model to  
581 simulate different logging practices (conventional and reduced impact) with various intensities.  
582 This newly developed selective logging module is capable of mimicking the ecological,  
583 biophysical, and biogeochemical processes at a landscape level following a logging event in a  
584 lumped way by (1) specifying the timing and areal extent of a logging event; (2) calculating the  
585 fractions of trees that are damaged by direct felling, collateral damage, and infrastructure damage,  
586 and adding these size-specific plant mortality types to FATES ; (3) splitting the logged patch into  
587 disturbed and intact new patches; (4) applying the calculated survivorship to cohorts in the  
588 disturbed patch; and (5) transporting harvested logs off-site and adding the remaining necromass  
589 from damaged trees into coarse woody debris and litter pools.

590 We then applied FATES coupled to CLM to the Tapajós National Forest by conducting  
591 numerical experiments driven by observed meteorological forcing, and benchmarked the  
592 simulations against long-term ecological and eddy covariance measurements. We demonstrated  
593 that the model is capable of simulating site-level water, energy, and carbon budgets, as well as



594 forest structure and composition holistically, with responses consistent with those documented in  
595 the existing literature as follows:

- 596 1. The model captures perturbations on energy and water budget terms in response to different  
597 levels of logging disturbances. Our modelling results suggest that logging leads to reductions  
598 in canopy interception, canopy evaporation and transpiration, as well as elevated soil  
599 temperature and soil heat fluxes in magnitudes proportional to the damage levels.
- 600 2. The logging disturbance leads to reductions in GPP, NPP, AR, and AGB, and increases in ER,  
601 NEE, HR, and CWD. The initial impacts of logging on the carbon budget are also proportional  
602 to damage levels as results of different logging practices.
- 603 3. Following the logging event, simulated carbon fluxes such as GPP, NPP, and AR recover  
604 within five years, but it takes decades for AGB to return to its pre-logging levels. Consistent  
605 with existing observational based literature, initial recovery of AGB is faster when the logging  
606 intensity is higher in response to improved light environment in the forest but the time to full  
607 AGB recovery in higher intensity logging is longer.
- 608 4. Consistent with observations at Tapajós, the prescribed logging event introduces a large  
609 amount of necromass to the forest floor proportional to the damage level of the logging event,  
610 which returns to pre-logging level in ~15 years. Simulated HR in low-damage reduced impact  
611 logging scenario stays elevated in five years following logging and declines to be the same as  
612 the intact forest in ~10 years.
- 613 5. The impacts of alternative logging practices on forest structure and composition were assessed  
614 by parameterizing cohort-specific mortality corresponding to direct felling, collateral damage,  
615 mechanical damage in the logging module to represent different logging practices (i.e.,  
616 conventional logging and reduced impact logging) and intensity (i.e., high and low). In all  
617 scenarios, the improved light environment after removal of large trees facilitates establishment  
618 and growth of early successional trees in the 0-10 cm DBH size class proportional to the  
619 damage levels in the first 2-3 year. Thereafter there is a transition to late successional trees in  
620 later years when the canopy is closed. The number of early successional trees then slowly  
621 declines but is sustained throughout the simulation as a result of natural disturbances.

622 Given that the representation of gas exchange processes is related to, but also somewhat  
623 independent of the representation of ecosystem demography, FATES shows great potential in its  
624 capability to capturing ecosystem successional processes in terms of gap-phase regeneration,



625 competition among light-demanding and shade-tolerant species following disturbance, as well as  
626 responses of energy, water, and carbon budget components to disturbances. The model projections  
627 suggest that while most degraded forests rapidly recover energy fluxes, the recovery times for  
628 carbon stocks, forest size structure and forest composition are much longer. The recovery  
629 trajectories are highly dependent on logging intensity and practices, the difference between which  
630 can be directly simulated by the model. Consistent with field studies, we find through numerical  
631 experiments that reduced impact logging leads to more rapid recovery of the water, energy, and  
632 carbon cycles, allowing forest structure and composition to recover to their pre-logging levels in a  
633 shorter time frame.

## 634 **5 Future work**

635 Currently, the selective logging module can only simulate single logging events. For regional-  
636 scale applications, it will be crucial to represent forest degradation as a result of logging, fire, and  
637 fragmentation and their combinations that could repeat over a period. Therefore, we will enable  
638 structural changes in FATES to track disturbance histories associated with fire, logging, and  
639 transitions among land use types. Nevertheless, this study lays the foundation to simulate land use  
640 change and forest degradation in FATES, leading the way to direct representation of forest  
641 management practices and regeneration in Earth System Models.

642 We also acknowledge that as a model development study, we applied the model to a site using  
643 a single set of parameter values and therefore we ignored the uncertainty associated with model  
644 parameters. We are also working on fixing the low LAI bias in the model. Preliminary testing  
645 suggests that by reducing the penalty for establishing leaf biomass, the low LAI bias could be  
646 significantly mitigated. This improvement will be evaluated in our follow-up studies.

647 In addition to the low LAI bias, it is clear that down-regulation factor to transpiration, the  
648 beta factor, is very low in the simulations, leading to underestimation of evapotranspiration and  
649 overestimation of sensible heat fluxes in the dry season. On-going efforts in developing more  
650 mechanistic plant hydraulic models (thereby eliminating the need for a beta factor) could  
651 potentially alleviate the problem (*Christofferson et al.* 2016) and will also be reported separately.

652





653 **Author contribution**

654 M.H., M.K., and M. L. conceived the study, conceptualized the design of the logging module, and  
655 designed the numerical experiments and analysis. Y. X., M. H., and R. K. coded the module. Y.  
656 X., R. K., C. K., R. F., M. H. integrated the module into FATES. M. H. performed the numerical  
657 experiments and wrote the manuscript with inputs from all coauthors.

658

659 **Acknowledgements**

660 This research was supported by The Next-Generation Ecosystem Experiments – Tropics project  
661 through the Terrestrial Ecosystem Science (TES) program within US Department of Energy’s  
662 Office of Biological and Environmental Research (BER). RF acknowledges the National Science  
663 Foundation via their support of the National Center for Atmospheric Research. M.L. was  
664 supported by the São Paulo State Research Foundation (FAPESP, grant 2015/07227-6).

665

666

667 **Code and data availability**

668 FATES-CLM has two separate repositories for FATES and CLM at:

669 [https://github.com/NGEET/fates/releases/tag/sci.1.6.0\\_api.3.0.0](https://github.com/NGEET/fates/releases/tag/sci.1.6.0_api.3.0.0)

670 <https://github.com/NGEET/fates-clm/releases>.

671 Site information and data at km67 and km83 can be found at <http://sites.fluxdata.org/BR-Sa1>  
672 and <http://sites.fluxdata.org/BR-Sa13>.

673 A README guide to run the model and formatted datasets used to drive model in this study will  
674 be made available from the open-source repository XXXXXX upon acceptance of the manuscript.

675

676

677 **References**

- 678 Asner, G. P., Keller, M., Pereira, J. R., Zweede, J. C., and Silva, J. N. M.: Canopy damage and recovery after selective logging in  
679 amazonia: field and satellite studies, *Ecological Applications*, 14, 280-298, 10.1890/01-6019, 2004.
- 680 Asner, G. P., Knapp, D. E., Broadbent, E. N., Oliveira, P. J. C., Keller, M., and Silva, J. N.: Selective Logging in the Brazilian  
681 Amazon, *Science*, 310, 480, 2005.
- 682 Asner, G.P., M. Keller, R. Pereira, and J.C. Zweed. 2008. LBA-ECO LC-13 GIS Coverages of Logged Areas, Tapajos Forest, Para,  
683 Brazil: 1996, 1998. ORNL DAAC, Oak Ridge, Tennessee, USA. <http://dx.doi.org/10.3334/ORNLDAAC/893>.
- 684 Asner, G. P., Rudel, T. K., Aide, T. M., Defries, R., and Emerson, R.: A Contemporary Assessment of Change in Humid Tropical  
685 Forests
- 686 Una Evaluación Contemporánea del Cambio en Bosques Tropicales Húmedos, *Conservation Biology*, 23, 1386-1395,  
687 10.1111/j.1523-1739.2009.01333.x, 2009.
- 688 Baidya Roy, S., Hurtt, G. C., Weaver, C. P., and Pacala, S. W.: Impact of historical land cover change on the July climate of the  
689 United States, *Journal of Geophysical Research: Atmospheres*, 108, n/a-n/a, 10.1029/2003JD003565, 2003.
- 690 Baker, I.T., Prihodko, L., Denning, A.S., Goulden, M., Miller, S. and Da Rocha, H.R. Seasonal drought stress in the Amazon:  
691 Reconciling models and observations. *Journal of Geophysical Research: Biogeosciences*, 113(G1),  
692 <https://doi.org/10.1029/2007JG000644>, 2008.
- 693 Baraloto, C., B. Hérault, C. E. T. Paine, H. Massot, L. Blanc, D. Bonal, J.-F. Molino, E. A. Nicolini, and D. Sabatier. Contrasting  
694 taxonomic and functional responses of a tropical tree community to selective logging. *J. Appl. Ecol.*, 49(4):861–870, Aug 2012.  
695 doi:10.1111/j.1365-2664.2012.02164.x.
- 696 Berenguer, E., Ferreira, J., Gardner, T. A., Aragão, L. E. O. C., De Camargo, P. B., Cerri, C. E., Durigan, M., Oliveira, R. C. D.,  
697 Vieira, I. C. G., and Barlow, J.: A large-scale field assessment of carbon stocks in human-modified tropical forests, *Global Change*  
698 *Biology*, 20, 3713-3726, 10.1111/gcb.12627, 2014.
- 699 Blaser, J., Sarre, A., Poore, D., and Johnson, S.: Status of Tropical Forest Management 2011. , International Tropical Timber  
700 Organization, Yokohama, Japan, 2011.
- 701 Bohn, K., Dyke, J.G., Pavlick, R., Reineking, B., Reu, B. and Kleidon, A.: The relative importance of seed competition, resource  
702 competition and perturbations on community structure. *Biogeosciences*, 8(5), 1107-1120, <https://doi.org/10.5194/bg-8-1107-2011>,  
703 2011.
- 704 Bonan, G. B.: Forests and Climate Change: Forcings, Feedbacks, and the Climate Benefits of Forests, *Science*, 320, 1444, 2008.
- 705 Bradshaw, C. J. A., Sodhi, N. S., and Brook, B. W.: Tropical turmoil: a biodiversity tragedy in progress, *Frontiers in Ecology and*  
706 *the Environment*, 7, 79-87, 10.1890/070193, 2009.
- 707 Both, S., T. Riutta, C. E. T. Paine, D. M. O. Elias, R. S. Cruz, A. Jain, D. Johnson, U. H. Kritzler, M. Kuntz, N. Majalap-Lee, N.  
708 Mielke, M. X. Montoya Pillco, N. J. Ostle, Y. Arn Teh, Y. Malhi, and D. F. R. P. Burslem. Logging and soil nutrients independently  
709 explain plant trait expression in tropical forests. *New Phytol.*, 2018. doi:10.1111/nph.15444.
- 710 Brando, P. M., Goetz, S. J., Baccini, A., Nepstad, D. C., Beck, P. S. A., and Christman, M. C.: Seasonal and interannual variability  
711 of climate and vegetation indices across the Amazon, *Proceedings of the National Academy of Sciences*, 107, 14685-14690,  
712 10.1073/pnas.0908741107, 2010.
- 713 Brokaw, N.: Gap-Phase Regeneration in a Tropical Forest, *Ecology*, 66, 682-687, 10.2307/1940529, 1985.
- 714 Bustamante, M. M. C., Roitman, I., Aide, T. M., Alencar, A., Anderson, L., Aragão, L., Asner, G. P., Barlow, J., Berenguer, E.,  
715 Chambers, J., Costa, M. H., Fanin, T., Ferreira, L. G., Ferreira, J. N., Keller, M., Magnusson, W. E., Morales, L., Morton, D.,  
716 Ometto, J. P. H. B., Palace, M., Peres, C., Silvério, D., Trumbore, S., and Vieira, I. C. G.: Towards an integrated monitoring  
717 framework to assess the effects of tropical forest degradation and recovery on carbon stocks and biodiversity, *Global Change*  
718 *Biology*, n/a-n/a, 10.1111/gcb.13087, 2015.
- 719 Chambers, J. Q., Tribuzy, E. S., Toledo, L. C., Crispim, B. F., Higuchi, N., Santos, J. d., Araújo, A. C., Kruijt, B., Nobre, A. D.,  
720 and Trumbore, S. E.: RESPIRATION FROM A TROPICAL FOREST ECOSYSTEM: PARTITIONING OF SOURCES AND  
721 LOW CARBON USE EFFICIENCY, *Ecological Applications*, 14, 72-88, 10.1890/01-6012, 2004.
- 722 Christoffersen, B. O., Gloor, M., Fauset, S., Fyllas, N. M., Galbraith, D. R., Baker, T. R., Kruijt, B., Rowland, L., Fisher, R. A.,  
723 Binks, O. J., Sevanto, S., Xu, C., Jansen, S., Choat, B., Mencuccini, M., McDowell, N. G., and Meir, P.: Linking hydraulic traits  
724 to tropical forest function in a size-structured and trait-driven model (TFS v.1-Hydro), *Geosci. Model Dev.*, 9, 4227-4255,  
725 10.5194/gmd-9-4227-2016, 2016.
- 726 de Gonçalves, L. G. G., Borak, J. S., Costa, M. H., Saleska, S. R., Baker, I., Restrepo-Coupe, N., Muza, M. N., Poulter, B.,  
727 Verbeeck, H., Fisher, J. B., Arain, M. A., Arkin, P., Cestaro, B. P., Christoffersen, B., Galbraith, D., Guan, X., van den Hurk, B. J.  
728 J. M., Ichii, K., Imbuzeiro, H. M. A., Jain, A. K., Levine, N., Lu, C., Miguez-Macho, G., Roberti, D. R., Sahoo, A., Sakaguchi, K.,  
729 Schaefer, K., Shi, M., Shuttleworth, W. J., Tian, H., Yang, Z.-L., and Zeng, X.: Overview of the Large-Scale Biosphere-  
730 Atmosphere Experiment in Amazonia Data Model Intercomparison Project (LBA-DMIP), *Agricultural and Forest Meteorology*,  
731 182-183, 111-127, <https://doi.org/10.1016/j.agrformet.2013.04.030>, 2013.
- 732 de Sousa, C.A.D., J.R. Elliot, E.L. Read, A.M.S. Figueira, S.D. Miller, and M.L. Goulden. 2011. LBA-ECO CD-04 Logging  
733 Damage, km 83 Tower Site, Tapajos National Forest, Brazil. ORNL DAAC, Oak Ridge, Tennessee, USA.  
734 <https://doi.org/10.3334/ORNLDAAC/1038Dirzo>, R., Young, H. S., Galetti, M., Ceballos, G., Isaac, N. J. B., and Collen, B.:  
735 Defaunation in the Anthropocene, *Science*, 345, 401-406, 10.1126/science.1251817, 2014.
- 736 Dlugokencky, E.J., Hall, B.D., Montzka, S.A., Dutton, G., Mühle, J., Elkins, J.W. 2018. Atmospheric composition [in *State of the*  
737 *Climate in 2017*]. *Bulletin of the American Meteorological Society*, 99(8), S46–S49.



- 738 Domingues, T. F., Berry, J. A., Martinelli, L. A., Ometto, J. P. H. B., and Ehleringer, J. R.: Parameterization of Canopy Structure  
739 and Leaf-Level Gas Exchange for an Eastern Amazonian Tropical Rain Forest (Tapajós National Forest, Pará, Brazil), *Earth*  
740 *Interactions*, 9, 1-23, 10.1175/ei149.1, 2005.
- 741 Doughty, C. E., and Goulden, M. L.: Seasonal patterns of tropical forest leaf area index and CO<sub>2</sub> exchange, *Journal of Geophysical*  
742 *Research: Biogeosciences*, 113, n/a-n/a, 10.1029/2007JG000590, 2008.
- 743 Dykstra, D. P.: Reduced impact logging: concepts and issues, *Applying Reduced Impact Logging to Advance Sustainable Forest*  
744 *Management*, 23-39, 2002.
- 745 Erb, K.-H., Kastner, T., Plutzer, C., Bais, A. L. S., Carvalhais, N., Fetzel, T., Gingrich, S., Haberl, H., Lauk, C., Niedertscheider,  
746 M., Pongratz, J., Thurner, M., and Luyssaert, S.: Unexpectedly large impact of forest management and grazing on global vegetation  
747 biomass, *Nature*, 553, 73, 10.1038/nature25138  
748 <https://www.nature.com/articles/nature25138#supplementary-information>, 2017.
- 749 Feldpausch, T. R., Jirka, S., Passos, C. A. M., Jasper, F., and Riha, S. J.: When big trees fall: Damage and carbon export by reduced  
750 impact logging in southern Amazonia, *Forest Ecology and Management*, 219, 199-215,  
751 <https://doi.org/10.1016/j.foreco.2005.09.003>, 2005.
- 752 Figueira, A. M. e. S., Miller, S. D., de Sousa, C. A. D., Menton, M. C., Maia, A. R., da Rocha, H. R., and Goulden, M. L.: Effects  
753 of selective logging on tropical forest tree growth, *Journal of Geophysical Research: Biogeosciences*, 113, n/a-n/a,  
754 10.1029/2007JG000577, 2008.
- 755 Fisher, R., McDowell, N., Purves, D., Moorcroft, P., Sitch, S., Cox, P., Huntingford, C., Meir, P., and Ian Woodward, F.: Assessing  
756 uncertainties in a second-generation dynamic vegetation model caused by ecological scale limitations, *New Phytologist*, 187, 666-  
757 681, 10.1111/j.1469-8137.2010.03340.x, 2010.
- 758 Fisher, R. A., Muszala, S., Versteinstein, M., Lawrence, P., Xu, C., McDowell, N. G., Knox, R. G., Koven, C., Holm, J., Rogers, B.  
759 M., Spessa, A., Lawrence, D., and Bonan, G.: Taking off the training wheels: the properties of a dynamic vegetation model without  
760 climate envelopes, *CLM4.5(ED)*, *Geosci. Model Dev.*, 8, 3593-3619, 10.5194/gmd-8-3593-2015, 2015.
- 761 Fisher, R. A., Koven, C. D., Anderegg, W. R. L., Christoffersen, B. O., Dietze, M. C., Farnior, C. E., Holm, J. A., Hurtt, G. C.,  
762 Knox, R. G., Lawrence, P. J., Lichstein, J. W., Longo, M., Matheny, A. M., Medvigy, D., Muller-Landau, H. C., Powell, T. L.,  
763 Serbin, S. P., Sato, H., Shuman, J. K., Smith, B., Trugman, A. T., Viskari, T., Verbeeck, H., Weng, E., Xu, C., Xu, X., Zhang, T.,  
764 and Moorcroft, P. R.: Vegetation demographics in Earth System Models: A review of progress and priorities, *Global Change*  
765 *Biology*, n/a-n/a, 10.1111/gcb.13910, 2017.
- 766 Foken, T.: THE ENERGY BALANCE CLOSURE PROBLEM: AN OVERVIEW, *Ecological Applications*, 18, 1351-1367,  
767 10.1890/06-0922.1, 2008.
- 768 Goulden, M. L., Miller, S. D., da Rocha, H. R., Menton, M. C., de Freitas, H. C., e Silva Figueira, A. M., and de Sousa, C. A. D.:  
769 DIEL AND SEASONAL PATTERNS OF TROPICAL FOREST CO<sub>2</sub> EXCHANGE, *Ecological Applications*, 14, 42-54,  
770 10.1890/02-6008, 2004.
- 771 Goulden, M.L., S.D. Miller, and H.R. da Rocha. 2010. LBA-ECO CD-04 Soil Moisture Data, km 83 Tower Site, Tapajós National  
772 Forest, Brazil. ORNL DAAC, Oak Ridge, Tennessee, USA. <https://doi.org/10.3334/ORNLDAAC/979>
- 773 Hayek, M. N., Wehr, R., Longo, M., Hutyra, L. R., Wiedemann, K., Munger, J. W., Bonal, D., Saleska, S. R., Fitzjarrald, D. R.,  
774 and Wofsy, S. C.: A novel correction for biases in forest eddy covariance carbon balance, *Agricultural and Forest Meteorology*,  
775 250-251, 90-101, <https://doi.org/10.1016/j.agrformet.2017.12.186>, 2018.
- 776 Huang, M., Asner, G. P., Keller, M., and Berry, J. A.: An ecosystem model for tropical forest disturbance and selective logging,  
777 *Journal of Geophysical Research: Biogeosciences*, 113, n/a-n/a, 10.1029/2007JG000438, 2008.
- 778 Huang, M., and Asner, G. P.: Long-term carbon loss and recovery following selective logging in Amazon forests, *Global*  
779 *Biogeochemical Cycles*, 24, n/a-n/a, 10.1029/2009GB003727, 2010.
- 780 Hurtt, G. C., Moorcroft, P. R., And, S. W. P., and Levin, S. A.: Terrestrial models and global change: challenges for the future,  
781 *Global Change Biology*, 4, 581-590, 10.1046/j.1365-2486.1998.t01-1-00203.x, 1998.
- 782 Hurtt, G. C., Chini, L. P., Frolking, S., Betts, R. A., Feddema, J., Fischer, G., Fisk, J. P., Hibbard, K., Houghton, R. A., Janetos,  
783 A., Jones, C. D., Kindermann, G., Kinoshita, T., Klein Goldewijk, K., Riahi, K., Shevliakova, E., Smith, S., Stehfest, E., Thomson,  
784 A., Thornton, P., van Vuuren, D. P., and Wang, Y. P.: Harmonization of land-use scenarios for the period 1500–2100: 600 years  
785 of global gridded annual land-use transitions, wood harvest, and resulting secondary lands, *Climatic Change*, 109, 117,  
786 10.1007/s10584-011-0153-2, 2011.
- 787 Keller, M., Palace, M., and Hurtt, G.: Biomass estimation in the Tapajós National Forest, Brazil: Examination of sampling and  
788 allometric uncertainties, *Forest Ecology and Management*, 154, 371-382, [https://doi.org/10.1016/S0378-1127\(01\)00509-6](https://doi.org/10.1016/S0378-1127(01)00509-6), 2001.
- 789 Keller, M., Alencar, A., Asner, G. P., Braswell, B., Bustamante, M., Davidson, E., Feldpausch, T., Fernandes, E., Goulden, M.,  
790 Kabat, P., Kruijt, B., Luizão, F., Miller, S., Markewitz, D., Nobre, A. D., Nobre, C. A., Priante Filho, N., da Rocha, H., Silva Dias,  
791 P., von Randow, C., and Vourlitis, G. L.: ECOLOGICAL RESEARCH IN THE LARGE-SCALE BIOSPHERE– ATMOSPHERE  
792 EXPERIMENT IN AMAZONIA: EARLY RESULTS, *Ecological Applications*, 14, 3-16, 10.1890/03-6003, 2004a.
- 793 Keller, M., Palace, M., Asner, G. P., Pereira, R., and Silva, J. N. M.: Coarse woody debris in undisturbed and logged forests in the  
794 eastern Brazilian Amazon, *Global Change Biology*, 10, 784-795, 10.1111/j.1529-8817.2003.00770.x, 2004b.
- 795 Keller, M., Varner, R., Dias, J. D., Silva, H., Crill, P., Jr., R. C. d. O., and Asner, G. P.: Soil–Atmosphere Exchange of Nitrous  
796 Oxide, Nitric Oxide, Methane, and Carbon Dioxide in Logged and Undisturbed Forest in the Tapajós National Forest, Brazil, *Earth*  
797 *Interactions*, 9, 1-28, 10.1175/ei125.1, 2005.



- 798 Knox, R. G., Longo, M., Swann, A. L. S., Zhang, K., Levine, N. M., Moorcroft, P. R., and Bras, R. L.: Hydrometeorological effects  
799 of historical land-conversion in an ecosystem-atmosphere model of Northern South America, *Hydrol. Earth Syst. Sci.*, 19, 241-  
800 273, 10.5194/hess-19-241-2015, 2015.
- 801 Longo, M., R. G. Knox, D. M. Medvigy, N. M. Levine, M. C. Dietze, Y. Kim, A. L. S. Swann, K. Zhang, C. R. Rollinson, , D.  
802 Bonal, B. Burban, P. B. Camargo, M. N. Hayek, S. R. Saleska, R. da Silva, R. L. Bras, S. C. Wofsy, and P. R. Moorcroft. The  
803 biophysics, ecology, and biogeochemistry of functionally diverse, vertically- and horizontally-heterogeneous ecosystems: the  
804 Ecosystem Demography model, version 2.2. Manuscript in review for *Geosci. Model Dev.*, 2019.
- 805 Lawrence, P. J., Feddema, J. J., Bonan, G. B., Meehl, G. A., O'Neill, B. C., Oleson, K. W., Levis, S., Lawrence, D. M., Kluzek,  
806 E., Lindsay, K., and Thornton, P. E.: Simulating the Biogeochemical and Biogeophysical Impacts of Transient Land Cover Change  
807 and Wood Harvest in the Community Climate System Model (CCSM4) from 1850 to 2100, *Journal of Climate*, 25, 3071-3095,  
808 10.1175/jcli-d-11-00256.1, 2012.
- 809 Leng G, LY Leung, and M Huang : Significant impacts of irrigation water sources and methods on modeling irrigation effects in  
810 the ACME Land Model. *J. Adv. Model. Earth Syst.* 9(3):1665 - 1683. doi:10.1002/2016MS000885. 2017.
- 811 Lloyd, J., Patiño, S., Paiva, R. Q., Nardoto, G. B., Quesada, C. A., Santos, A. J. B., Baker, T. R., Brand, W. A., Hilke, I., Gielmann,  
812 H., Raessler, M., Luizão, F. J., Martinelli, L. A., and Mercader, L. M.: Optimisation of photosynthetic carbon gain and within-  
813 canopy gradients of associated foliar traits for Amazon forest trees, *Biogeosciences*, 7, 1833-1859, <https://doi.org/10.5194/bg-7-1833-2010>, 2010.
- 814 Longo, M., R. G. Knox, N. M. Levine, L. F. Alves, D. Bonal, P. B. Camargo, D. R. Fitzjarrald, M. N. Hayek, N. Restrepo-Coupe,  
815 S. R. Saleska, R. da Silva, S. C. Stark, R. P. Tapajós, K. T. Wiedemann, K. Zhang, S. C. Wofsy, and P. R. Moorcroft. Ecosystem  
816 heterogeneity and diversity mitigate Amazon forest resilience to frequent extreme droughts. *New Phytol.*, 219(3):914–931, Aug  
817 2018. doi:10.1111/nph.
- 818 Luyssaert, S., Schulze, E. D., Börner, A., Knohl, A., Hessenmoller, D., Law, B. E., Ciais, P., and Grace, J.: Old-growth forests as  
819 global carbon sinks, *Nature*, 455, 213-215, [http://www.nature.com/nature/journal/v455/n7210/supinfo/nature07276\\_S1.html](http://www.nature.com/nature/journal/v455/n7210/supinfo/nature07276_S1.html),  
820 2008.
- 821 Macpherson, A. J., Carter, D. R., Schulze, M. D., Vidal, E., and Lentini, M. W.: The sustainability of timber production from  
822 Eastern Amazonian forests, *Land Use Policy*, 29, 339-350, <https://doi.org/10.1016/j.landusepol.2011.07.004>, 2012.
- 823 Martínez-Ramos, M., Ortiz-Rodríguez, I. A., Piñero, D., Dirzo, R., and Sarukhán, J.: Anthropogenic disturbances jeopardize  
824 biodiversity conservation within tropical rainforest reserves, *Proceedings of the National Academy of Sciences*, 113, 5323-5328,  
825 10.1073/pnas.1602893113, 2016.
- 826 Massoud, E. C., Xu, C., Fisher, R., Knox, R., Walker, A., Serbin, S., Christoffersen, B., Holm, J., Kueppers, L., Ricciuto, D. M.,  
827 Wei, L., Johnson, D., Chambers, J., Koven, C., McDowell, N., and Vrugt, J.: Identification of key parameters controlling  
828 demographically structured vegetation dynamics in a Land Surface Model [CLM4.5(ED)], *Geosci. Model Dev. Discuss.*,  
829 <https://doi.org/10.5194/gmd-2019-6>, in review, 2019.
- 830 Mazzei, L., Sist, P., Ruschel, A., Putz, F. E., Marco, P., Pena, W., and Ferreira, J. E. R.: Above-ground biomass dynamics after  
831 reduced-impact logging in the Eastern Amazon, *Forest Ecology and Management*, 259, 367-373,  
832 <https://doi.org/10.1016/j.foreco.2009.10.031>, 2010.
- 833 Medvigy, D., Wofsy, S. C., Munger, J. W., Hollinger, D. Y., and Moorcroft, P. R.: Mechanistic scaling of ecosystem function and  
834 dynamics in space and time: Ecosystem Demography model version 2, *Journal of Geophysical Research: Biogeosciences*, 114, n/a-  
835 n/a, 10.1029/2008JG000812, 2009.
- 836 Menton, M.C., A.M.S. Figueira, C.A.D. de Sousa, S.D. Miller, H.R. da Rocha, and M.L. Goulden. 2011. LBA-ECO CD-04  
837 Biomass Survey, km 83 Tower Site, Tapajos National Forest, Brazil. ORNL DAAC, Oak Ridge, Tennessee, USA.  
838 <https://doi.org/10.3334/ORNLDAAC/990>
- 839 Miller, S. D., Goulden, M. L., Menton, M. C., da Rocha, H. R., de Freitas, H. C., Figueira, A. M. e. S., and Dias de Sousa, C. A.:  
840 BIOMETRIC AND MICROMETEOROLOGICAL MEASUREMENTS OF TROPICAL FOREST CARBON BALANCE,  
841 *Ecological Applications*, 14, 114-126, 10.1890/02-6005, 2004.
- 842 Miller, S. D., Goulden, M. L., Hutrya, L. R., Keller, M., Saleska, S. R., Wofsy, S. C., Figueira, A. M. S., da Rocha, H. R., and de  
843 Camargo, P. B.: Reduced impact logging minimally alters tropical rainforest carbon and energy exchange, *Proceedings of the*  
844 *National Academy of Sciences of the United States of America*, 108, 19431-19435, 10.1073/pnas.1105068108, 2011.
- 845 Moorcroft, P. R., Hurtt, G. C., and Pacala, S. W.: A METHOD FOR SCALING VEGETATION DYNAMICS: THE ECOSYSTEM  
846 DEMOGRAPHY MODEL (ED), *Ecological Monographs*, 71, 557-586, 10.1890/0012-9615(2001)071[0557:AMFSDV]2.0.CO;2,  
847 2001.
- 848 Morton, D. C., Nagol, J., Carabjal, C. C., Rosette, J., Palace, M., Cook, B. D., Vermote, E. F., Harding, D. J., and North, P. R. J.:  
849 Amazon forests maintain consistent canopy structure and greenness during the dry season, *Nature*, 506, 221, 10.1038/nature13006  
850 <https://www.nature.com/articles/nature13006#supplementary-information>, 2014.
- 851 Nepstad, D. C., Verssimo, A., Alencar, A., Nobre, C., Lima, E., Lefebvre, P., Schlesinger, P., Potter, C., Moutinho, P., Mendoza,  
852 E., Cochrane, M., and Brooks, V.: Large-scale impoverishment of Amazonian forests by logging and fire, *Nature*, 398, 505-508,  
853 1999.
- 854 Oleson, K. W., Lawrence, D. M., Bonan, G. B., Drewniak, B., Huang, M., Koven, C. D., Levis, S., Li, F., Riley, W. J., Subin, Z.  
855 M., Swenson, S. C., Thornton, P. E., Bozbiyik, A., Fisher, R., Kluzek, E., Lamarque, J.-F., Lawrence, P. J., Leung, L. R., Lipscomb,  
856 W., Muszala, S., Ricciuto, D. M., Sacks, W., Sun, Y., Tang, J., and Yang, Z.-L.: Technical Description of version 4.5 of the  
857 Community Land Model (CLM), National Center for Atmospheric Research, Boulder, CONcar Technical Note NCAR/TN-  
858 503+STR, 2013.



- 860 Palace, M., Keller, M., and Silva, H.: NECROMASS PRODUCTION: STUDIES IN UNDISTURBED AND LOGGED AMAZON  
861 FORESTS, *Ecological Applications*, 18, 873-884, 10.1890/06-2022.1, 2008.
- 862 Pan, Y., Birdsey, R. A., Fang, J., Houghton, R., Kauppi, P. E., Kurz, W. A., Phillips, O. L., Shvidenko, A., Lewis, S. L., Canadell,  
863 J. G., Ciais, P., Jackson, R. B., Pacala, S. W., McGuire, A. D., Piao, S., Rautiainen, A., Sitch, S., and Hayes, D.: A Large and  
864 Persistent Carbon Sink in the World's Forests, *Science*, 333, 988-993, 2011.
- 865 Pearson, T., Brown, S., and Casarim, F.: Carbon emissions from tropical forest degradation caused by logging, *Environmental*  
866 *Research Letters*, 9, 034017, 2014.
- 867 Pereira Jr, R., Zweede, J., Asner, G. P., and Keller, M.: Forest canopy damage and recovery in reduced-impact and conventional  
868 selective logging in eastern Para, Brazil, *Forest Ecology and Management*, 168, 77-89, [http://dx.doi.org/10.1016/S0378-  
869 1127\(01\)00732-0](http://dx.doi.org/10.1016/S0378-1127(01)00732-0), 2002.
- 870 Piponiot C, Derroire G, Descroix L, Mazzei L, Rutishauser E, Sist P, Hérault B. 2018. Assessing timber volume  
871 recovery after disturbance in tropical forests – a new modelling framework. *Ecol. Model.*, 384: 353–369.  
872 doi:10.1016/j.ecolmodel.2018.05.023.
- 873 Powell, T.L., Galbraith, D.R., Christoffersen, B.O., Harper, A., Imbuzeiro, H.M., Rowland, L., Almeida, S., Brando, P.M., da  
874 Costa, A.C.L., Costa, M.H. and Levine, N.M., 2013. Confronting model predictions of carbon fluxes with measurements of Amazon  
875 forests subjected to experimental drought. *New Phytologist*, 200(2), pp.350-365.
- 876 Putz, F. E., Sist, P., Fredericksen, T., and Dykstra, D.: Reduced-impact logging: Challenges and opportunities, *Forest Ecology and*  
877 *Management*, 256, 1427-1433, <https://doi.org/10.1016/j.foreco.2008.03.036>, 2008.
- 878 Reich, P. B.: The world-wide 'fast-slow' plant economics spectrum: a traits manifesto, *Journal of Ecology*, 102(2), 275-301,  
879 <https://doi.org/10.1111/1365-2745.12211>, 2014.
- 880 Rice, A. H., Pyle, E. H., Saleska, S. R., Hutyra, L., Palace, M., Keller, M., de Camargo, P. B., Portilho, K., Marques, D. F., and  
881 Wofsy, S. C.: CARBON BALANCE AND VEGETATION DYNAMICS IN AN OLD-GROWTH AMAZONIAN FOREST,  
882 *Ecological Applications*, 14, 55-71, 10.1890/02-6006, 2004.
- 883 Rutishauser, E., Hérault, B., Baraloto, C., Blanc, L., Descroix, L., Sotta, E.D., Ferreira, J., Kanashiro, M., Mazzei, L., d'Oliveira,  
884 M.V. and De Oliveira, L.C., 2015. Rapid tree carbon stock recovery in managed Amazonian forests. *Current Biology*, 25(18),  
885 pp.R787-R788. Saleska, S. R., Miller, S. D., Matross, D. M., Goulden, M. L., Wofsy, S. C., da Rocha, H. R., de Camargo, P. B.,  
886 Crill, P., Daube, B. C., de Freitas, H. C., Hutyra, L., Keller, M., Kirchoff, V., Menton, M., Munger, J. W., Pyle, E. H., Rice, A.  
887 H., and Silva, H.: Carbon in Amazon Forests: Unexpected Seasonal Fluxes and Disturbance-Induced Losses, *Science*, 302, 1554,  
888 2003.
- 889 Saleska, S.R., H.R. da Rocha, A.R. Huete, A.D. Nobre, P. Artaxo, and Y.E. Shimabukuro. 2013. LBA-ECO CD-32 Flux Tower  
890 Network Data Compilation, Brazilian Amazon: 1999-2006. Data set. Available on-line [<http://daac.ornl.gov>] from Oak Ridge  
891 National Laboratory Distributed Active Archive Center, Oak Ridge, Tennessee,  
892 USA <http://dx.doi.org/10.3334/ORNLDAAAC/1174>.
- 893 Saleska, S. R., Wu, J., Guan, K., Araujo, A. C., Huete, A., Nobre, A. D., and Restrepo-Coupe, N.: Dry-season greening of Amazon  
894 forests, *Nature*, 531, E4, 10.1038/nature16457, 2016.
- 895 Sato, H., Itoh, A., and Kohyama, T.: SEIB-DGVM: A new Dynamic Global Vegetation Model using a spatially explicit individual-  
896 based approach, *Ecological Modelling*, 200, 279-307, <https://doi.org/10.1016/j.ecolmodel.2006.09.006>, 2007.
- 897 Shevliakova, E., Pacala, S. W., Malyshev, S., Hurtt, G. C., Milly, P. C. D., Caspersen, J. P., Sentman, L. T., Fisk, J. P., Wirth, C.,  
898 Crevoisier, C., Carbon cycling under 300 years of land use change: Importance of the secondary vegetation sink, *Global*  
899 *biogeochemical cycles*, 2009, 23(2), <https://doi.org/10.1029/2007GB003176>.
- 900 Silver, W. L., Neff, J., McGroddy, M., Veldkamp, E., Keller, M., and Cosme, R.: Effects of Soil Texture on Belowground Carbon  
901 and Nutrient Storage in a Lowland Amazonian Forest Ecosystem, *Ecosystems*, 3, 193-209, 10.1007/s10021000019, 2000.
- 902 Sist, P., Rutishauser, E., Peña-Claros, M., Shenkin, A., Hérault, B., Blanc, L., Baraloto, C., Baya, F., Benedet, F., da Silva, K. E.,  
903 Descroix, L., Ferreira, J. N., Gourlet-Fleury, S., Guedes, M. C., Bin Harun, I., Jalonen, R., Kanashiro, M., Krisnawati, H., Kshatriya,  
904 M., Lincoln, P., Mazzei, L., Medjibé, V., Nasi, R., d'Oliveira, M. V. N., de Oliveira, L. C., Picard, N., Pietsch, S., Pinard, M.,  
905 Priyadi, H., Putz, F. E., Rodney, K., Rossi, V., Roopsind, A., Ruschel, A. R., Shari, N. H. Z., Rodrigues de Souza, C., Susanty, F.  
906 H., Sotta, E. D., Toledo, M., Vidal, E., West, T. A. P., Wortel, V., and Yamada, T.: The Tropical managed Forests Observatory: a  
907 research network addressing the future of tropical logged forests, *Applied Vegetation Science*, 18, 171-174, 10.1111/avsc.12125,  
908 2015.
- 909 Smith, B., Prentice, I. C., and Sykes, M. T.: Representation of vegetation dynamics in the modelling of terrestrial ecosystems:  
910 comparing two contrasting approaches within European climate space, *Global Ecology and Biogeography*, 10, 621-637,  
911 10.1046/j.1466-822X.2001.t01-1-00256.x, 2001.
- 912 Smith, B., Wårlind, D., Arneth, A., Hickler, T., Leadley, P., Siltberg, J., and Zaehle, S.: Implications of incorporating N cycling  
913 and N limitations on primary production in an individual-based dynamic vegetation model, *Biogeosciences*, 11, 2027-2054,  
914 10.5194/bg-11-2027-2014, 2014.
- 915 Strigul, N., Pristiniski, D., Purves, D., Dushoff, J., and Pacala, S.: SCALING FROM TREES TO FORESTS: TRACTABLE  
916 MACROSCOPIC EQUATIONS FOR FOREST DYNAMICS, *Ecological Monographs*, 78, 523-545, 10.1890/08-0082.1, 2008.
- 917 Thonicke, K., Spessa, A., Prentice, I. C., Harrison, S. P., Dong, L., and Carmona-Moreno, C.: The influence of vegetation, fire  
918 spread and fire behaviour on biomass burning and trace gas emissions: results from a process-based model, *Biogeosciences*, 7,  
919 1991-2011, 10.5194/bg-7-1991-2010, 2010.
- 920 Tomasella, J. and Hodnett, M.G., 1998. Estimating soil water retention characteristics from limited data in Brazilian Amazonia.  
921 *Soil science*, 163(3), pp.190-202.





- 922 Trumbore, S., and Barbosa De Camargo, P.: Soil carbon dynamics, Amazonia and global change, 451-462, 2009.
- 923 Watanabe, S., Hajima, T., Sudo, K., Nagashima, T., Takemura, T., Okajima, H., Nozawa, T., Kawase, H., Abe, M., Yokohata, T.,
- 924 Ise, T., Sato, H., Kato, E., Takata, K., Emori, S., and Kawamiya, M.: MIROC-ESM 2010: model description and basic results of
- 925 CMIP5-20c3m experiments, *Geosci. Model Dev.*, 4, 845-872, [10.5194/gmd-4-845-2011](https://doi.org/10.5194/gmd-4-845-2011), 2011.
- 926 Weng, E. S., Malyshev, S., Lichstein, J. W., Farrior, C. E., Dybzinski, R., Zhang, T., Shevliakova, E., and Pacala, S. W.: Scaling
- 927 from individual trees to forests in an Earth system modeling framework using a mathematically tractable model of height-structured
- 928 competition, *Biogeosciences*, 12, 2655-2694, [10.5194/bg-12-2655-2015](https://doi.org/10.5194/bg-12-2655-2015), 2015.
- 929 Whitmore, T. C.: *An Introduction to Tropical Rain Forests*, OUP Oxford, 1998.
- 930 Wilson, K., Goldstein, A., Falge, E., Aubinet, M., Baldocchi, D., Berbigier, P., Bernhofer, C., Ceulemans, R., Dolman, H., Field,
- 931 C., Grelle, A., Ibrom, A., Law, B. E., Kowalski, A., Meyers, T., Moncrieff, J., Monson, R., Oechel, W., Tenhunen, J., Valentini,
- 932 R., and Verma, S.: Energy balance closure at FLUXNET sites, *Agricultural and Forest Meteorology*, 113, 223-
- 933 243, [http://dx.doi.org/10.1016/S0168-1923\(02\)00109-0](http://dx.doi.org/10.1016/S0168-1923(02)00109-0), 2002.
- 934 Wright, I. J., Reich, P. B., Westoby, M., and Ackerly, D. D.: The worldwide leaf economics spectrum, *Nature*, 428, 821, 2004.
- 935 Wu, J., Albert, L.P., Lopes, A.P., Restrepo-Coupe, N., Hayek, M., Wiedemann, K.T., Guan, K., Stark, S.C., Christoffersen, B.,
- 936 Prohaska, N. and Tavares, J.V., 2016. Leaf development and demography explain photosynthetic seasonality in Amazon evergreen
- 937 forests. *Science*, 351(6276), pp.972-976
- 938 Wu, J. K. Guan, M. Hayek, N. Restrepo-Coupe, K.T. Wiedemann, X. Xu, R. Wehr, B.O. Christoffersen, G. Miao, R. da Silva, A.C.
- 939 de Araujo, R.C. Oliveira. P. B. Camargo, R. K. Monson, A.R. Huete, S.R. Saleska, Partitioning controls on Amazon forest
- 940 photosynthesis between environmental and biotic factors at hourly to interannual timescales, *Global change biology*, 23(3), 1240-
- 941 1257, <https://doi.org/10.1111/gcb.13509>, 2017.
- 942
- 943



1 **Tables and Figures**

2

3 Table 1. FATES Parameters that define early and late successional PFTs

Parameter names	Units	Early successional PFT	Late successional PFT
Specific leaf area	$\text{m}^2 \text{gC}^{-1}$	0.016	0.015
$V_{\text{cmax}}$ at 25°C	$\mu\text{mol m}^{-2} \text{s}^{-1}$	68	60
Specific wood density	$\text{g cm}^{-3}$	0.5	0.9
Leaf longevity	yr	0.9	2.6
Background mortality rate	$\text{yr}^{-1}$	0.035	0.014
Leaf C:N	$\text{gC gN}^{-1}$	20	40
root longevity	yr	0.9	2.6

4





5 Table 2. Distributions of stem density ( $\text{N ha}^{-1}$ ), basal area ( $\text{m}^2 \text{ha}^{-1}$ ) and above ground biomass ( $\text{Kg C m}^{-2}$ )  
 6 before and after logging at km83, separated by diameter of breast height (normal text) and aggregated across  
 7 all sizes (bold text).

Time	Before logging			After Logging		
Variables	Early	Late	<b>Total</b>	Early	Late	<b>Total</b>
<b>Stem Density (<math>\text{N ha}^{-1}</math>)</b>	<b>264</b>	<b>195</b>	<b>459</b>	<b>260</b>	<b>191</b>	<b>443</b>
Stem Density (10-30 cm, $\text{N ha}^{-1}$ )	230	169	<b>399</b>	229	167	<b>396</b>
Stem Density (30-50 cm, $\text{N ha}^{-1}$ )	18	12	<b>30</b>	17	12	<b>29</b>
Stem Density ( $\geq 50$ cm, $\text{N ha}^{-1}$ )	16	14	<b>30</b>	14	12	<b>18</b>
<b>Basal Area (<math>\text{m}^2 \text{ha}^{-1}</math>)</b>	<b>11.6</b>	<b>9.2</b>	<b>21.0</b>	<b>10.3</b>	<b>8.3</b>	<b>18.5</b>
Basal Area (10-30 cm, $\text{m}^2 \text{ha}^{-1}$ )	2.2	1.7	<b>4.2</b>	2.2	1.7	<b>3.8</b>
Basal Area (30-50 cm, $\text{m}^2 \text{ha}^{-1}$ )	2.4	1.6	<b>4.2</b>	2.4	1.6	<b>3.9</b>
Basal Area ( $\geq 50$ cm, $\text{m}^2 \text{ha}^{-1}$ )	7.0	5.9	<b>12.6</b>	5.8	5.1	<b>10.8</b>
<b>AGB (<math>\text{Kg C m}^{-2}</math>)</b>	<b>7.6</b>	<b>8.9</b>	<b>16.5</b>	<b>6.8</b>	<b>7.9</b>	<b>14.7</b>
AGB (10-30 cm, $\text{Kg C m}^{-2}$ )	1.8	2.0	<b>3.8</b>	1.8	2.0	<b>3.8</b>
AGB (30-50 cm, $\text{Kg C m}^{-2}$ )	1.1	1.1	<b>2.3</b>	1.1	1.1	<b>2.2</b>
AGB ( $\geq 50$ cm, $\text{Kg C m}^{-2}$ )	4.6	5.8	<b>10.4</b>	3.8	4.9	<b>8.7</b>

8 \* based on inventory during the LBA period (Menton *et al.*, 2011; de Sousa *et al.*, 2011)



9

10 Table 3. Cohort-level fractional damage fractions in different logging scenarios

Scenarios	Conventional Logging		Reduced Impact Logging	
	High	Low	High (KM83×2)	Low (KM83)
Experiments	CL <sub>high</sub>	CL <sub>low</sub>	RIL <sub>high</sub>	RIL <sub>low</sub>
Direct felling fraction (DBH ≥ DBH <sub>min</sub> <sup>1</sup> )	0.18	0.09	0.24	0.12
Collateral damage fraction (DBH ≥ DBH <sub>min</sub> )	0.036	0.018	0.024	0.012
mechanical damage fraction (DBH < DBH <sub>max_infra</sub> <sup>2</sup> )	0.113	0.073	0.033	0.024
Understory death fraction <sup>3</sup>	0.65	0.65	0.65	0.65

11 <sup>1</sup>DBH<sub>min</sub> = 50 cm

12 <sup>2</sup>DBH<sub>max\_infra</sub> = 30 cm

13 <sup>3</sup>Applied to the new patch generated by direct felling and collateral damage



- 14 Table 4. Comparison of energy fluxes (Mean  $\pm$  Standard Deviation) between eddy covariance  
15 tower measurements and FATES simulations.

Variables	LH ( $\text{W m}^{-2}$ )	SH ( $\text{W m}^{-2}$ )	Rn ( $\text{W m}^{-2}$ )
<b>Observed (km83)</b>	<b>101.6<math>\pm</math>8.0</b>	<b>25.6<math>\pm</math>5.2</b>	<b>129.3<math>\pm</math>18.5</b>
Simulated (Intact)	108.6 $\pm$ 21.0	20.1 $\pm$ 24.7	128.8 $\pm$ 15.6
<b>Simulated (RIL<sub>low</sub>)</b>	<b>108.3<math>\pm</math>20.8</b>	<b>20.5<math>\pm</math>24.3</b>	<b>128.9<math>\pm</math>15.5</b>
Simulated (RIL <sub>high</sub> )	108.0 $\pm$ 20.5	20.9 $\pm$ 23.9	129.0 $\pm$ 15.4
Simulated (CL <sub>low</sub> )	108.3 $\pm$ 20.8	20.5 $\pm$ 24.3	128.9 $\pm$ 15.5
Simulated (CL <sub>high</sub> )	108.0 $\pm$ 20.5	20.5 $\pm$ 24.3	129.0 $\pm$ 15.4

16



17

18 Table 5. Comparison of carbon budget terms between observation-based estimates\* and  
19 simulations at km83

Variable	Obs.		Simulated								
	Pre-logging	3-yr Post-logging	Intact	Disturb level	0 yr	1 yr	3 yr	15 yr	30 yr	50 yr	70 yr
AGB (MgC ha <sup>-1</sup> )	165	147	155	RIL <sub>low</sub>	138	138	140	143	146	150	155
				RIL <sub>high</sub>	119	120	122	127	133	141	147
				CL <sub>low</sub>	138	138	139	143	145	149	153
				CL <sub>high</sub>	119	119	121	128	133	140	146
Necromass (MgC ha <sup>-1</sup> )	58.4	74.4	41.1	RIL <sub>low</sub>	59.6	55.3	48.5	41.2	41.0	41.4	41.4
				RIL <sub>high</sub>	79.5	70.3	56.9	41.2	39.8	39.4	41.6
				CL <sub>low</sub>	60.0	55.4	48.7	41.0	40.9	40.9	41.1
				CL <sub>high</sub>	80.1	70.6	57.2	40.3	39.3	40.7	41.0
NEE (MgC ha <sup>-1</sup> yr <sup>-1</sup> )	-0.6±0.8	-1.0±0.7	0.49	RIL <sub>low</sub>	0.54	1.76	1.53	0.57	0.23	0.22	0.33
				RIL <sub>high</sub>	0.59	3.94	2.62	0.64	0.15	0.08	0.26
				CL <sub>low</sub>	0.54	1.83	1.55	0.56	0.24	0.31	0.44
				CL <sub>high</sub>	0.59	4.09	2.66	0.59	0.07	0.16	0.28
GPP (MgC ha <sup>-1</sup> yr <sup>-1</sup> )	32.6±1.3	32.0±1.3	17.6	RIL <sub>low</sub>	17.5	16.7	17.9	17.3	17.7	17.2	17.2
				RIL <sub>high</sub>	17.3	15.7	17.9	17.5	17.9	17.3	17.2
				CL <sub>low</sub>	17.5	16.6	17.9	17.3	17.7	17.3	17.2
				CL <sub>high</sub>	17.3	15.4	17.8	17.6	18.0	17.3	17.2
NPP (MgC ha <sup>-1</sup> yr <sup>-1</sup> )	9.5	9.8	8.9	RIL <sub>low</sub>	8.9	8.6	9.2	8.6	9.0	8.7	8.6
				RIL <sub>high</sub>	8.9	8.1	9.3	8.8	9.1	8.7	8.7
				CL <sub>low</sub>	8.9	8.5	9.2	8.7	9.0	8.6	8.6
				CL <sub>high</sub>	8.9	7.9	9.3	8.7	9.1	8.7	8.7
ER (MgC ha <sup>-1</sup> yr <sup>-1</sup> )	31.9±1.7	31.0±1.6	18.1	RIL <sub>low</sub>	18.0	18.6	19.6	17.9	18.0	17.5	17.5
				RIL <sub>high</sub>	17.9	19.6	21.2	18.2	18.1	17.3	17.5
				CL <sub>low</sub>	18.0	18.6	19.6	17.9	18.0	17.5	17.7
				CL <sub>high</sub>	17.9	19.5	21.2	18.2	18.0	17.4	17.5
HR (MgC ha <sup>-1</sup> yr <sup>-1</sup> )	8.9	10.4	9.4	RIL <sub>low</sub>	9.4	10.5	10.9	9.2	9.3	8.9	8.9
				RIL <sub>high</sub>	9.5	12.0	12.6	9.4	9.3	8.8	8.9
				CL <sub>low</sub>	9.4	10.5	11.0	9.2	9.3	8.9	9.0
				CL <sub>high</sub>	9.5	12.0	12.6	9.3	9.2	8.9	9.0
AR (MgC ha <sup>-1</sup> yr <sup>-1</sup> )	23.1	20.1	8.7	RIL <sub>low</sub>	8.6	8.1	8.7	8.7	8.7	8.5	8.6
				RIL <sub>high</sub>	8.4	7.6	8.6	8.8	8.8	8.6	8.6
				CL <sub>low</sub>	8.5	8.1	8.7	8.7	8.7	8.5	8.7
				CL <sub>high</sub>	8.4	7.5	8.6	8.9	8.8	8.5	8.6

20 \*Source of observation-based estimates: Miller et al. (2011), Uncertainty in carbon fluxes (GPP, ER, NEE) are based  
21 on u\*-filter cutoff analyses described in the same paper.



22

23 Table 6. Simulated Stem Density (N ha<sup>-1</sup>) Distribution at km83.

Years following logging	Disturbance level	Size classes (DBH, cm)			
		< 10 cm	10-30 cm	30-50 cm	≥ 50 cm
Pre-logging	Intact	9737	145	43	44
0-yr	RIL <sub>low</sub>	9203	143	43	38
	RIL <sub>high</sub>	8813	142	43	32
	CL <sub>low</sub>	8694	138	43	38
	CL <sub>high</sub>	8012	134	43	32
1-yr	RIL <sub>low</sub>	9072	147	28	51
	RIL <sub>high</sub>	9113	146	28	45
	CL <sub>low</sub>	9159	143	28	51
	CL <sub>high</sub>	9083	139	28	45
3-yr	RIL <sub>low</sub>	9909	139	25	47
	RIL <sub>high</sub>	11010	136	27	41
	CL <sub>low</sub>	9676	121	25	47
	CL <sub>high</sub>	10659	115	28	41
15-yr	RIL <sub>low</sub>	8609	161	66	37
	RIL <sub>high</sub>	8526	188	66	33
	CL <sub>low</sub>	6698	171	64	37
	CL <sub>high</sub>	8787	248	62	33
30-yr	RIL <sub>low</sub>	9277	90	68	33
	RIL <sub>high</sub>	9225	118	90	31
	CL <sub>low</sub>	8132	140	69	33
	CL <sub>high</sub>	10128	101	85	31
50-yr	RIL <sub>low</sub>	6995	132	64	54
	RIL <sub>high</sub>	8196	129	16	62
	CL <sub>low</sub>	8336	125	21	55
	CL <sub>high</sub>	7487	110	59	59
70-yr	RIL <sub>low</sub>	7904	128	55	52
	RIL <sub>high</sub>	6248	83	11	67
	CL <sub>low</sub>	9352	149	31	58
	CL <sub>high</sub>	6589	202	31	55

24

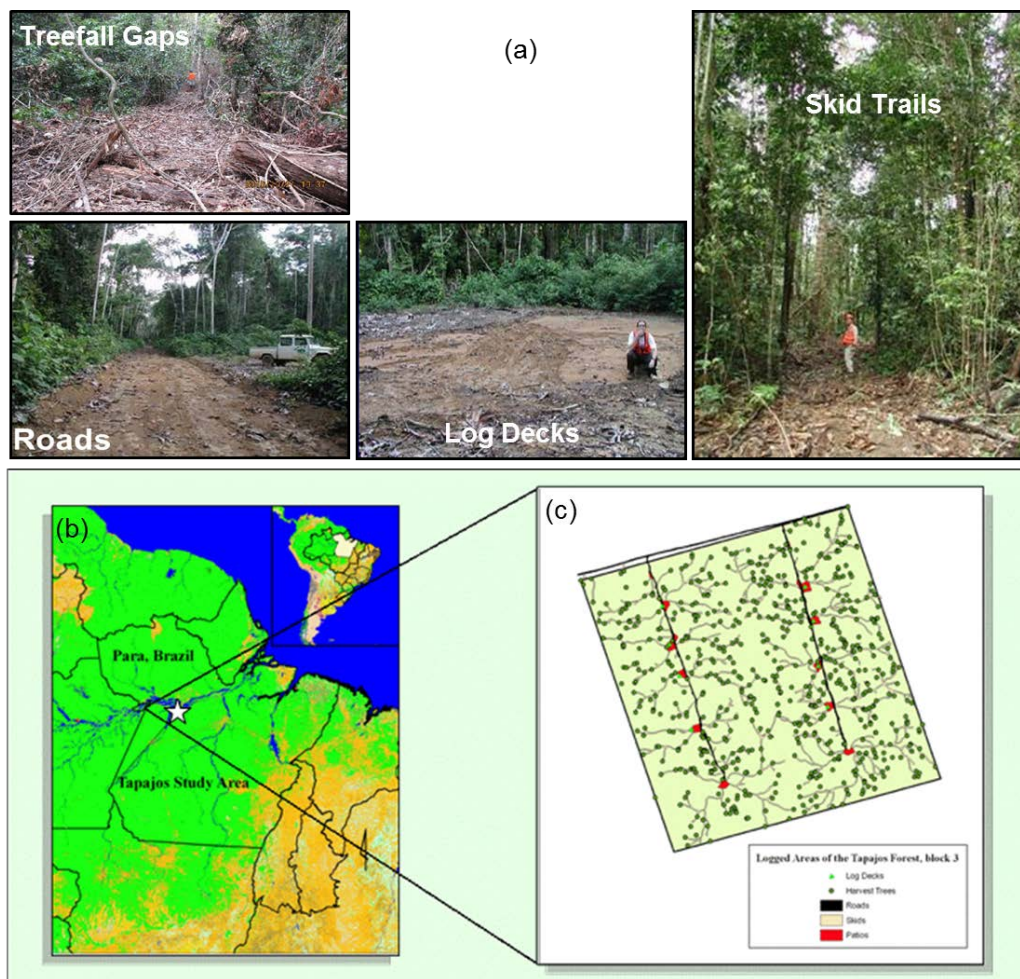


25 Table 7. Simulated Basal Area ( $m^2 ha^{-1}$ ) Distribution at km83.

Years following logging	Disturbance level	Size classes (DBH, cm)			
		< 10 cm	10-30 cm	30-50 cm	≥ 50 cm
Pre-logging	Intact	0.9	3.4	5.3	41.6
0-yr	RIL <sub>low</sub>	0.9	3.3	5.2	36.3
	RIL <sub>high</sub>	0.8	3.3	5.2	30.5
	CL <sub>low</sub>	0.8	3.2	5.3	36.3
	CL <sub>high</sub>	0.8	3.2	5.3	30.5
1-yr	RIL <sub>low</sub>	0.7	3.7	2.5	38.9
	RIL <sub>high</sub>	0.7	3.7	2.5	33.1
	CL <sub>low</sub>	0.8	3.6	2.5	38.9
	CL <sub>high</sub>	0.8	3.5	2.5	33.1
3-yr	RIL <sub>low</sub>	1.1	4.3	2.6	38.4
	RIL <sub>high</sub>	1.4	4.2	2.7	32.7
	CL <sub>low</sub>	1.3	4.0	2.6	38.4
	CL <sub>high</sub>	1.6	3.7	2.8	32.7
15-yr	RIL <sub>low</sub>	0.7	3.6	7.0	36.3
	RIL <sub>high</sub>	1.1	4.1	6.9	31.2
	CL <sub>low</sub>	0.6	3.8	6.8	36.4
	CL <sub>high</sub>	0.6	5.0	6.6	31.2
30-yr	RIL <sub>low</sub>	1.1	3.1	8.3	35.6
	RIL <sub>high</sub>	1.0	2.6	10.3	31.2
	CL <sub>low</sub>	0.8	3.5	8.3	35.6
	CL <sub>high</sub>	1.1	3.1	9.7	31.2
50-yr	RIL <sub>low</sub>	0.4	2.2	6.1	40.5
	RIL <sub>high</sub>	0.7	5.0	2.2	39.3
	CL <sub>low</sub>	1.0	4.6	2.9	40.7
	CL <sub>high</sub>	0.6	2.3	5.5	38.5
70-yr	RIL <sub>low</sub>	0.5	2.2	6.5	41.6
	RIL <sub>high</sub>	1.2	4.0	1.0	42.4
	CL <sub>low</sub>	0.7	3.6	3.0	42.9
	CL <sub>high</sub>	0.4	4.1	3.8	40.1

26

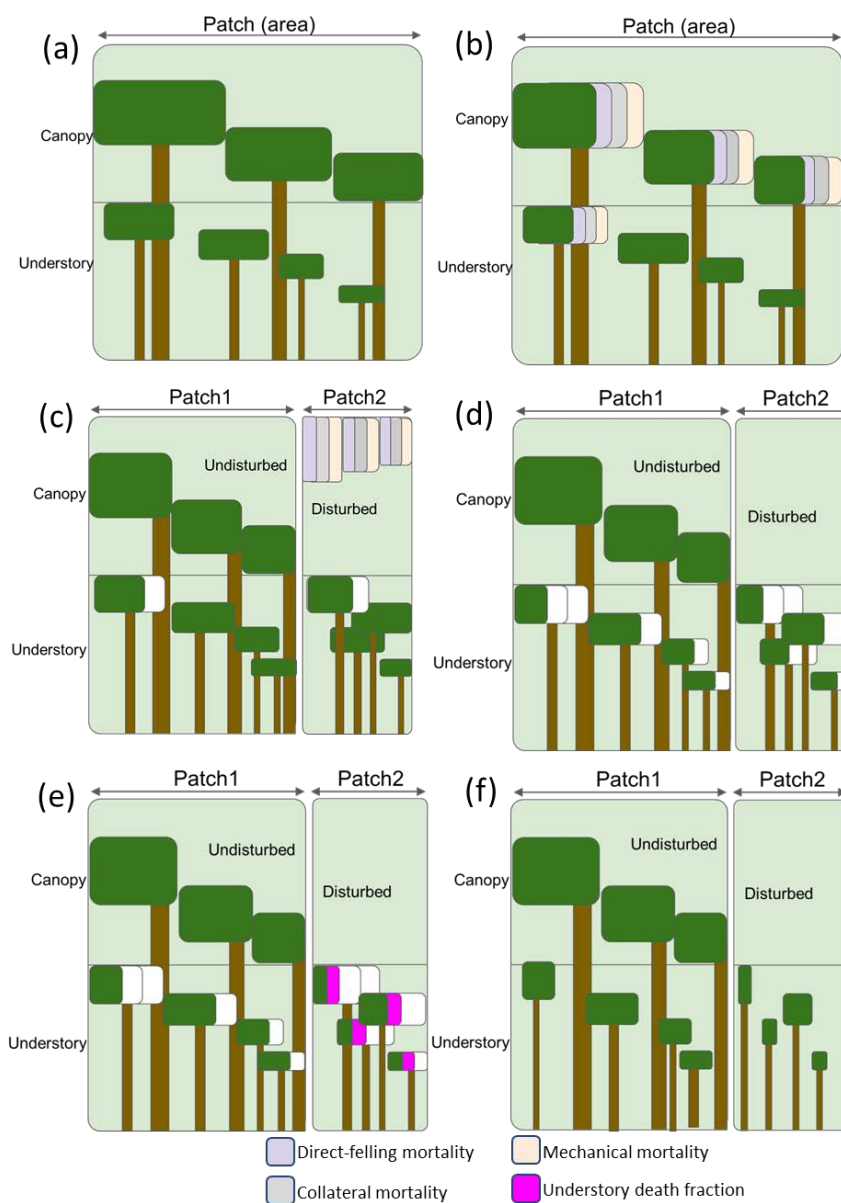
27



28

29 Figure 1. (a) Landscape components of selective logging; (b) location of the Tapajos National Forest in the  
30 Amazon; and (c) a typical logging block showing tree-fall location, skid trail, road, and log deck coverages.  
31 Panels (b) and (c) are from *Asner et al.* (2008).  
32



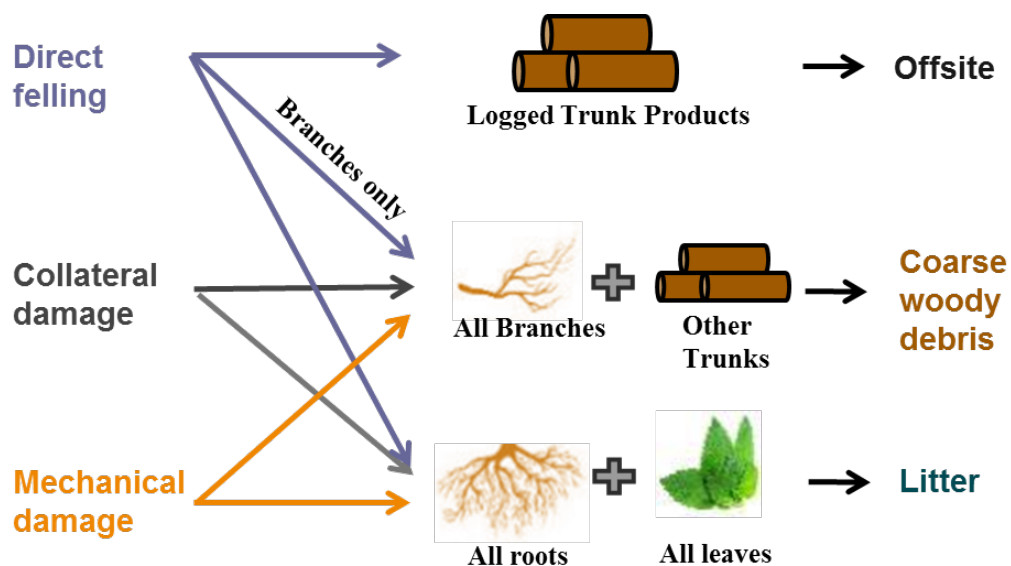


33

34 Figure 2. The mortality types (direct-felling, mechanical, and collateral) and patch generating process in  
 35 the FATES logging module. The white fraction in (c), (d), (f) indicates mortality associated with other  
 36 disturbances in FATES. (a) Canopy and understory layers in each cohort in FATES; (b) Mortality applied  
 37 at the time of a logging event; (c) the patch fission process following a given logging event; (d) canopy  
 38 removal in the disturbed patch following the logging event; (e) calculate the understory survivorship based  
 39 on the understory death fraction in each patch; (f) the final states of the intact and disturbed patches.  
 40



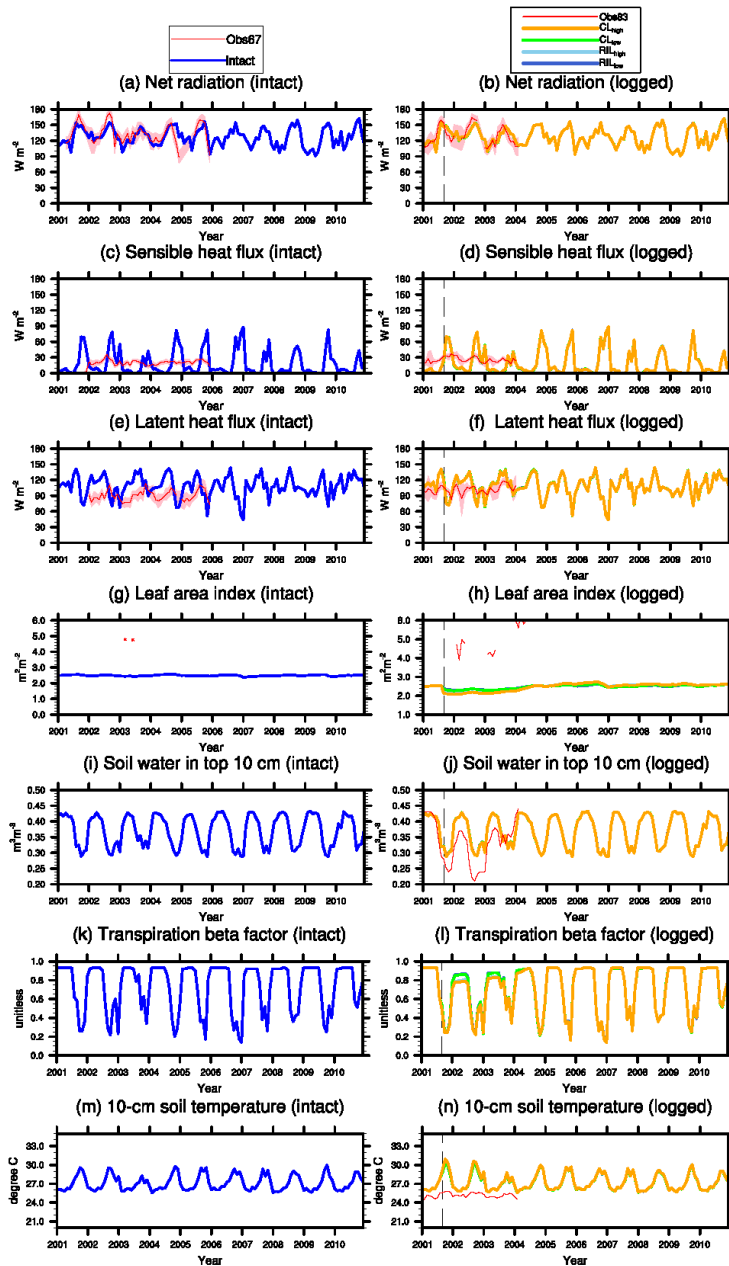
41



42

43 Figure 3. The flow of necromass following logging.

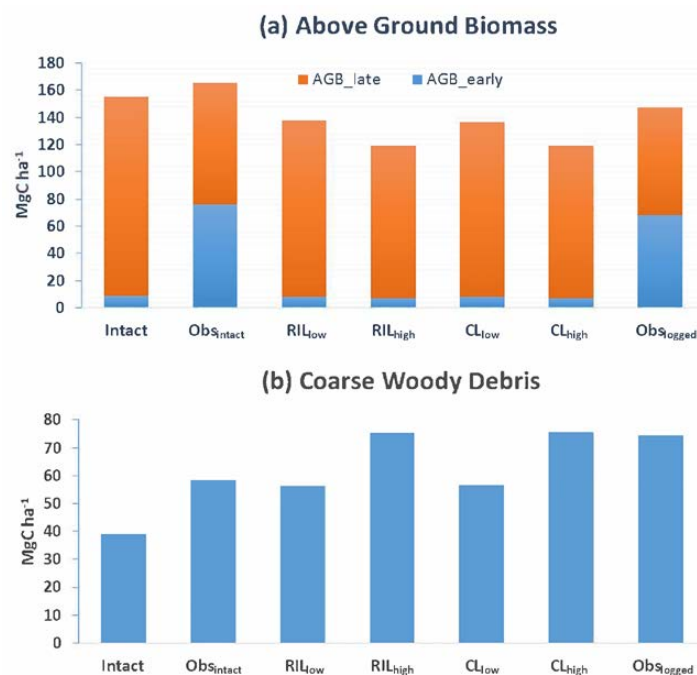
44



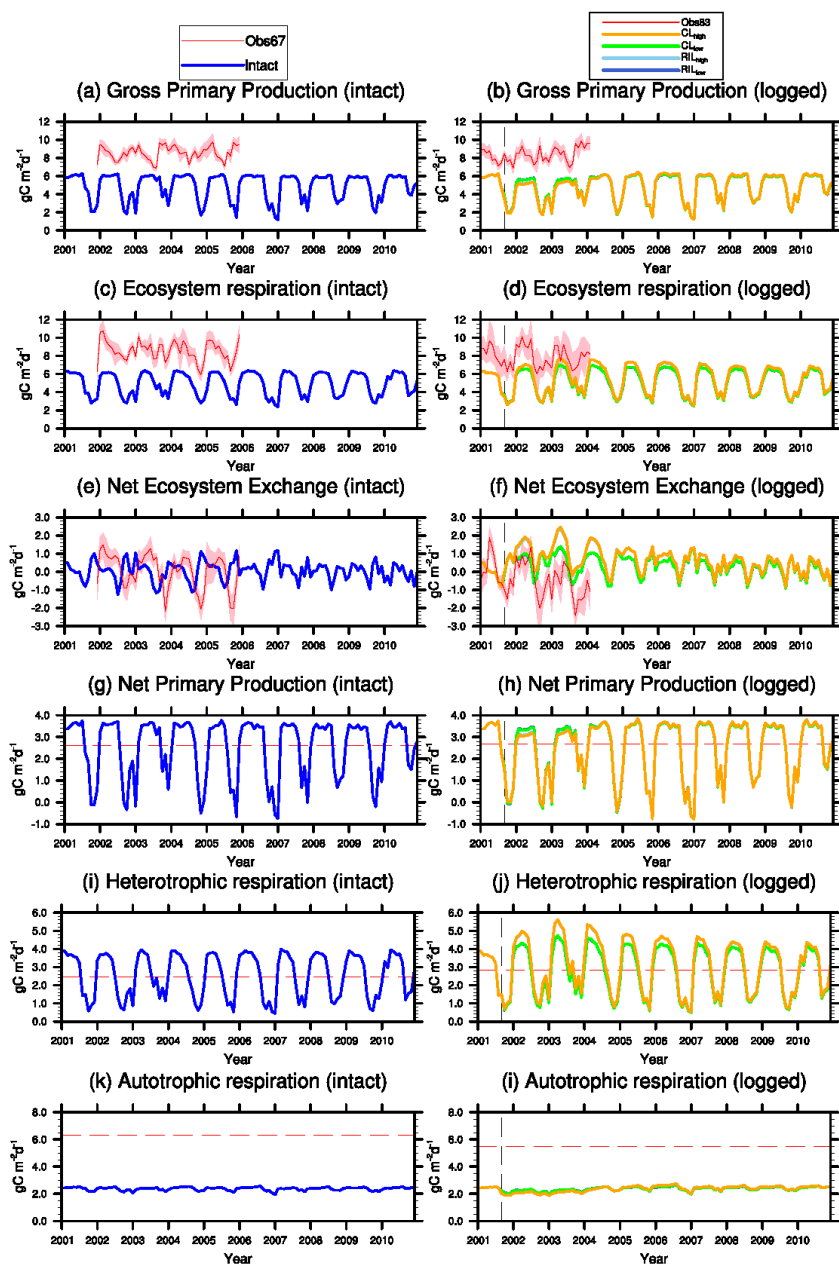
45

46 Figure 4. Simulated energy budget terms and leaf area indices in intact and logged forests compared to  
 47 observations from km67 (left) and km83 (right) (Miller *et al.*, 2011). The dashed vertical line indicates the  
 48 timing of the logging event. The shaded area in panel (a)-(f) are uncertainty estimates based on based on  
 49  $u^*$ -filter cutoff analyses in Miller *et al.* (2011).

50



51 Figure 5. Simulated (a) Above Ground Biomass; and (b) Coarse Woody Debris in intact and logged forests  
 52 in a one-year period before or after the logging event in the four logging scenarios listed in Table 3. The  
 53 observations (Obs<sub>intact</sub> and Obs<sub>logged</sub>) were derived from inventory (Menton *et al.*, 2011; de Sousa *et al.*,  
 54 2011).  
 55  
 56

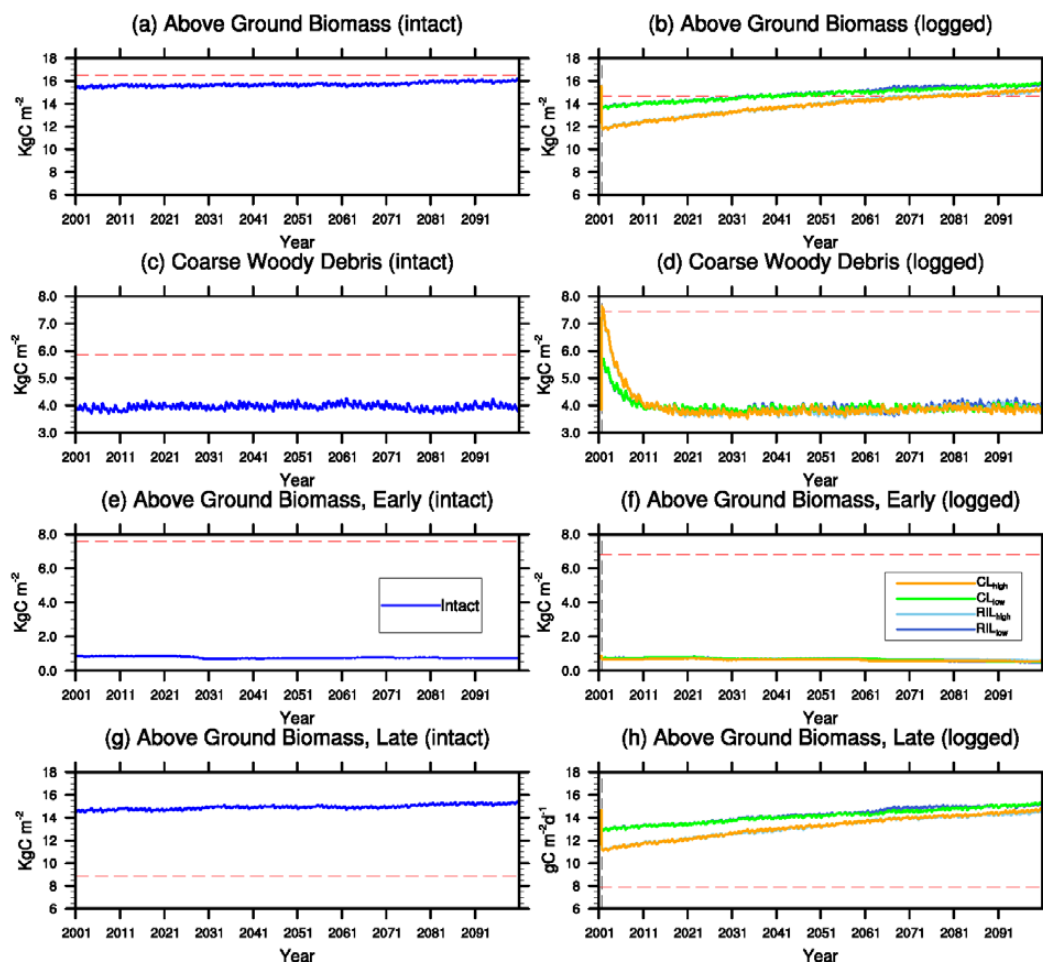


57

58 Figure 6. Simulated carbon fluxes in intact and logged forests compared to observed fluxes from km67  
 59 (left) and km83 (right). The dashed black vertical line indicates the timing of the logging event, while the  
 60 red dashed horizontal line indicates estimated fluxes derived based on eddy covariance measurements and  
 61 inventory (Miller *et al.*, 2011). The shaded area in panel (a)–(f) are uncertainty estimates based on  
 62  $u^*$ -filter cutoff analyses in Miller *et al.* (2011).  
 63

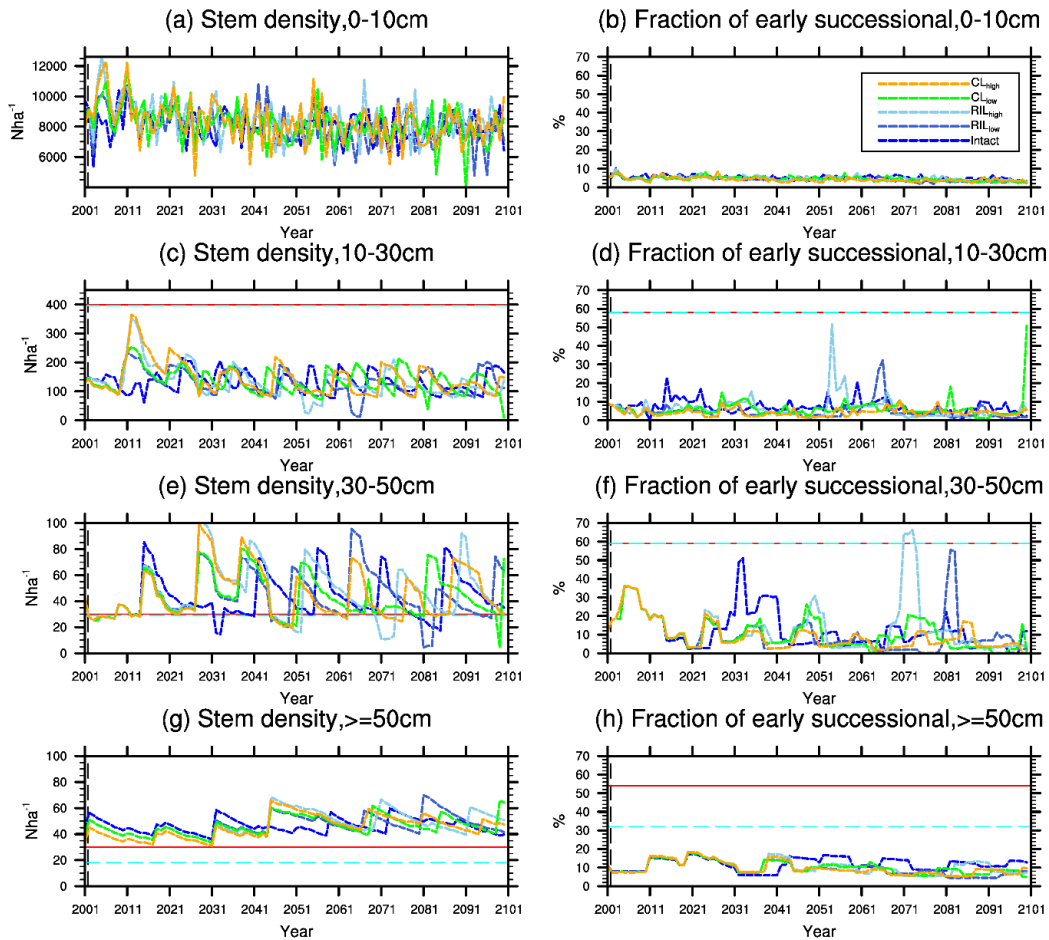


64



65

66 Figure 7. Trajectories of carbon pools in intact (left) and logged (right) forests. The dashed black vertical  
 67 line indicates the timing of the logging event. The red dashed horizontal line indicates observed pre- (left)  
 68 and post-logging (right) inventories respectively (*Menton et al., 2011*; *de Sousa et al., 2011*).  
 69



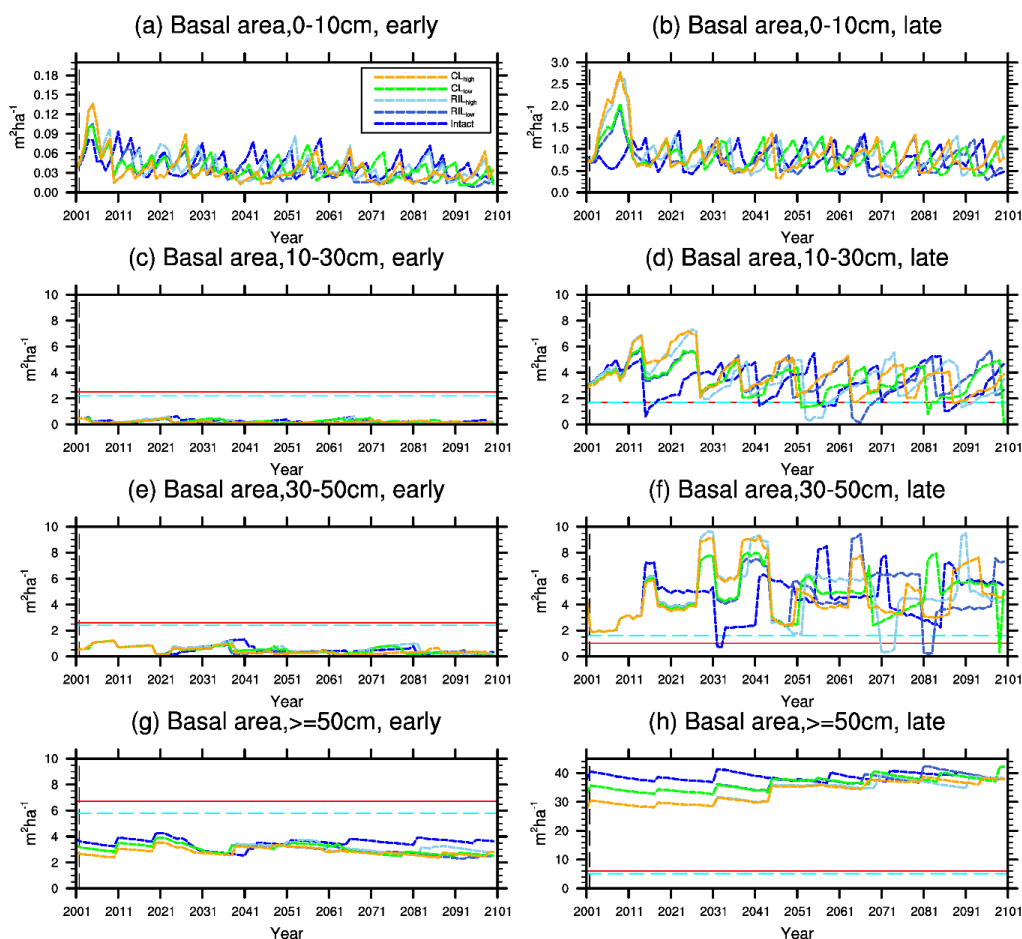
70

71 Figure 8. Changes in total stem densities and the fractions of the early successional PFT in different size  
72 classes following a single logging event on 1 September 2001 at km83. The black dashed vertical line  
73 indicates the timing of the logging event, while the red solid line and the cyan dashed horizontal line indicate  
74 observed pre- and post-logging inventories respectively (*Menton et al., 2011; de Sousa et al., 2011*).

75

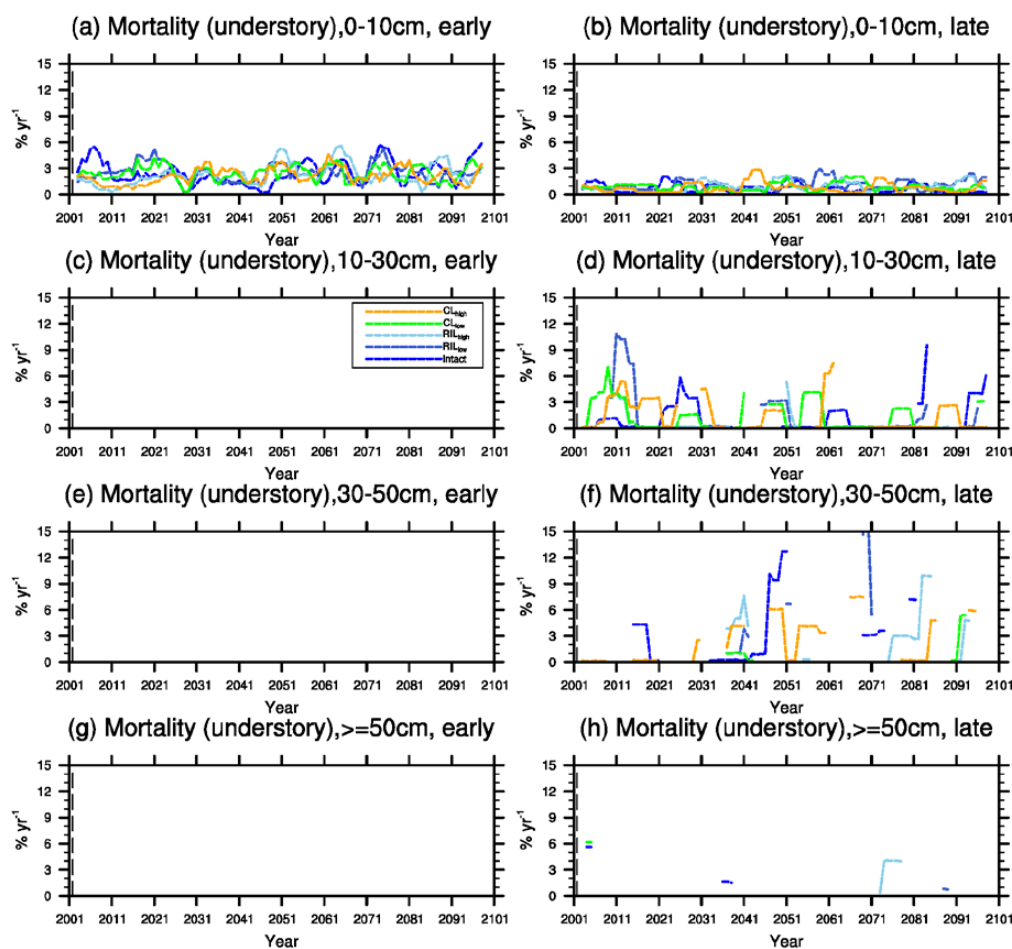
76



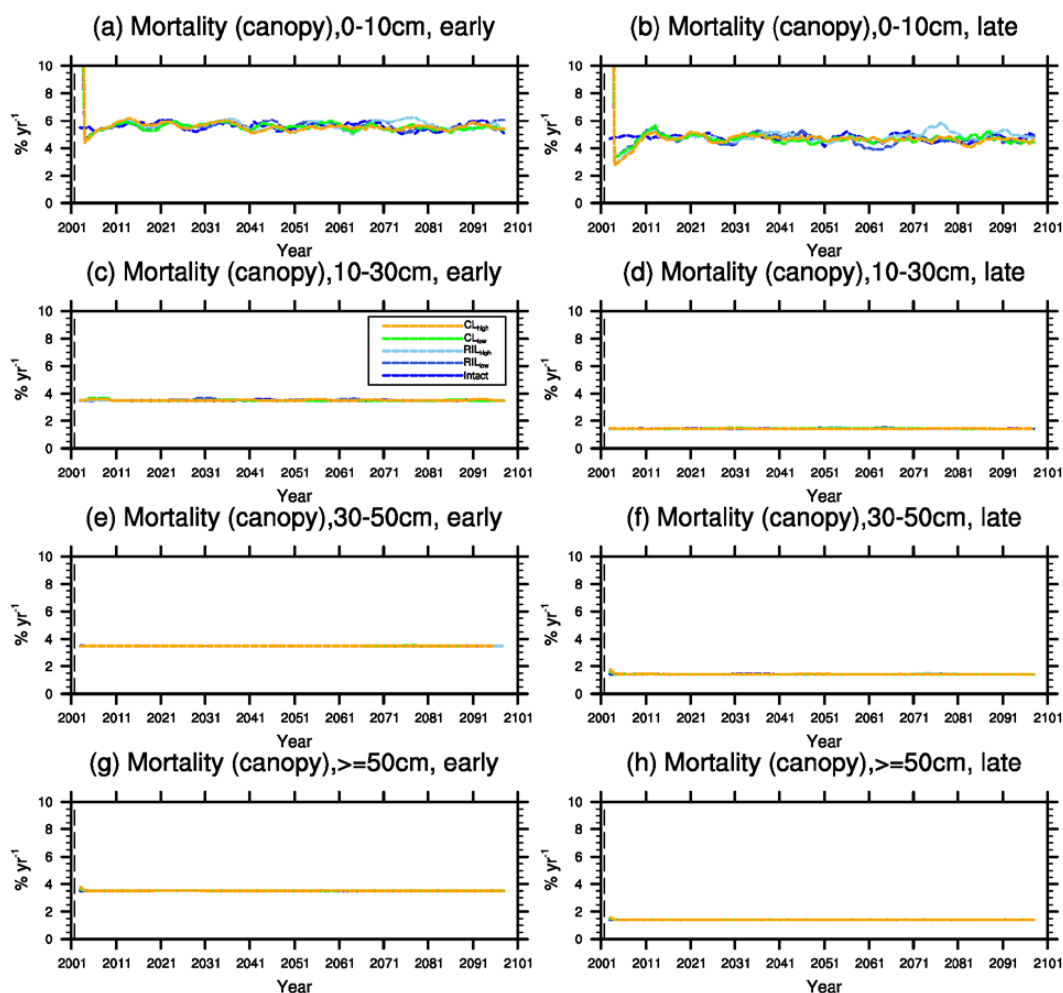


77

78 Figure 9. Changes in basal area of the two PFTs in different size classes following a single logging event  
 79 on 1 September 2001 at km83. The black dashed vertical line indicates the timing of the logging event,  
 80 while the red solid line and the cyan dashed horizontal line indicates observed pre- and post-logging  
 81 inventories respectively (Menton *et al.*, 2011; de Sousa *et al.*, 2011). Note that for the size class 0-10 cm,  
 82 observations are not available from the inventory.



83  
84 Figure 10. Changes in mortality (5-yr running average) of the understory trees in different size classes  
85 following a single logging event on 1 September 2001. The black dashed vertical line indicates the timing  
86 of the logging event. Note that mortality is not defined in large size classes because no tree survives in the  
87 understory or effectively promoted as canopy trees, especially for the early successional PFT.  
88



89  
 90 Figure 11. Changes in mortality (5-yr running average) of the canopy trees in different size classes  
 91 following a single logging event on 1 September 2001. The black dashed vertical line indicates the timing  
 92 of the logging event.  
 93